Paleoceanography and Paleoclimatology

RESEARCH ARTICLE
10.1029/2019PA003613

Key Points:
- New foraminifer ^{14}C records are presented, spanning from 540 to 3,100 m water depth along the Chilean Margin
- Waters at ~2,000 m were between 50% and 80% more depleted in $\Delta^{14}C$ than waters at ~1,500 m when compared to modern values
- Intermediate water records suggest that during the deglaciation, there was a deeper penetration of Antarctic Intermediate Water in the Pacific

Supporting Information:
- Supporting Information S1
- Table S1
- Table S2

Correspondence to:
R. De Pol-Holz,
ricardo.depol@umag.cl

Citation:
Martínez Fontaine, C., De Pol-Holz, R., Michel, E., Siani, G., Reyes-Macaya, D., Martínez-Méndez, G., et al. (2019). Ventilation of the deep ocean carbon reservoir during the last deglaciation: results from the southeast pacific. *Paleoceanography and Paleoclimatology*, *34*, 2080–2097. https://doi.org/10.1029/2019PA003613

Received 26 MAR 2019
Accepted 9 OCT 2019
Accepted article online 7 NOV 2019
Published online 19 DEC 2019

Ventilation of the Deep Ocean Carbon Reservoir During the Last Deglaciation: Results From the Southeast Pacific

Consuelo Martínez Fontaine[1,3,4], Ricardo De Pol-Holz[2], Elisabeth Michel[3], Giuseppe Siani[4], Dharma Reyes-Macaya[5], Gema Martínez-Méndez[5], Tim DeVries[6], Lowell Stott[7], John Southon[8], Mahyar Mohtadi[5], and Dierk Hebbeln[5]

[1]Departamento de Geología, Universidad de Chile, Santiago, Chile, [2]Centro de Investigación GAIA-Antárctica (CIGA) and Network for Extreme Environments Research (NEXER), Universidad de Magallanes, Punta Arenas, Chile, [3]Laboratoire des Sciences du Climat et de l'Environnement (LSCE), Laboratoire mixte CNRS-CEA, Gif-sur-Yvette Cedex, France, [4]Geoscience Paris Sud (GEOPS) Universities of Paris Sud and Paris-Saclay, CNRS, Orsay, France, [5]MARUM, Center for Marine Environmental Sciences, University of Bremen, Bremen, Germany, [6]Earth Research Institute, University of California, Santa Barbara, CA, USA, [7]Department of Earth Sciences, University of Southern California, Los Angeles, CA, USA, [8]Earth System Science Department, University of California, Irvine, CA, USA

Abstract Coeval changes in atmospheric CO_2 and ^{14}C contents during the last deglaciation are often attributed to ocean circulation changes that released carbon stored in the deep ocean during the Last Glacial Maximum (LGM). Work is being done to generate records that allow for the identification of the exact mechanisms leading to the accumulation and release of carbon from the oceanic reservoir, but these mechanisms are still the subject of debate. Here we present foraminifera ^{14}C data from five cores in a transect across the Chilean continental margin between ~540 and ~3,100 m depth spanning the last 20,000 years. Our data reveal that during the LGM, waters at ~2,000 m were 50% to 80% more depleted in $\Delta^{14}C$ than waters at ~1,500 m when compared to modern values, consistent with the hypothesis of a glacial deep ocean carbon reservoir that was isolated from the atmosphere. During the deglaciation, our intermediate water records reveal homogenization in the $\Delta^{14}C$ values between ~800 and ~1,500 m from ~16.5–14.5 ka cal BP to ~14–12 ka cal BP, which we interpret as deeper penetration of Antarctic Intermediate Water. While many questions still remain, this process could aid the ventilation of the deep ocean at the beginning of the deglaciation, contributing to the observed ~40 ppm rise in atmospheric pCO_2.

1. Introduction

The ocean is thought to play an important role in the variations of atmospheric pCO_2 over glacial-interglacial cycles. During the last deglaciation, a ~75 ppm rise in atmospheric pCO_2 (Barnola et al., 1987; Marcott et al., 2014; Monnin et al., 2001) occurred synchronously with a ~190 ± 10‰ drop in atmospheric $\Delta^{14}C$ (Reimer et al., 2013). Due to its large content of mobile carbon and the time scale of its overturning, the deep ocean is considered the most likely source of a ^{14}C-depleted CO_2 reservoir that would be transferred to the atmosphere during the last deglaciation (Broecker & Barker, 2007). Different hypotheses have been called upon to explain the ocean's role in changing atmospheric CO_2 concentrations and for the exact source area and mechanism controlling this release of depleted $^{14}CO_2$. Among these are changes in oceanic circulation leading to the formation of an isolated deepwater carbon reservoir (Adkins, 2013; Ferrari et al., 2014; Keeling & Stephens, 2001, Keeling, 2007; Toggweiler, 1999; Stephens & Keeling, 2000; Watson & Naveira Garabato, 2006), changes in the biological pump efficiency in capturing atmospheric CO_2 (e.g., Duchamp-Alphonse et al., 2018; Kohfeld et al., 2005; Pichevin et al., 2009; Sigman & Boyle, 2000), release of ^{14}C-dead CO_2 from clathrate deposits due to changes in the temperature of the ocean (Stott & Timmermann, 2011), and increased production of ^{14}C-dead CO_2 associated with higher magmatism in ocean ridges during periods of low sea level, such as the last glacial period (Crowley et al., 2015; Lund & Asimow, 2011; Tolstoy, 2015).

Evidence of the deep ocean as the source of the atmospheric ^{14}C decline has been found in marine sediment cores throughout the oceans. Widespread evidence of moderately ^{14}C-depleted deep waters (>2,000-m depth) during the late glacial period (25–10 ka BP) has been found in the North Pacific (NP; Galbraith

10.1029/2019PA003613

et al., 2007; Rae et al., 2014), South West Pacific (SWP; Ronge et al., 2016; Sikes et al., 2016), Equatorial East Pacific (EEP; De la Fuente et al., 2015; Keigwin & Lehman, 2015; Umling & Thunell, 2017), and Southern Ocean (SO; Burke & Robinson, 2012; Chen et al., 2015; Skinner et al., 2010). These records are consistent with the hypothesis of an isolated deep ocean reservoir during the Last Glacial Maximum (LGM) associated with increased sea ice extent around Antarctica (Adkins, 2013; Ferrari et al., 2014; Keeling & Stephens, 2001; Stephens & Keeling, 2000; Watson & Naveira Garabato, 2006). Additionally, extremely ^{14}C-depleted values have been found in deepwater sediment cores dating from the LGM in the SWP (Ronge et al., 2016; Sikes et al., 2016; Skinner et al., 2015) and East Pacific Rise (EPR; Ronge et al., 2016) and during the deglaciation in intermediate water cores in the EEP (Bova et al., 2018; Stott et al., 2009), Baja California (Lindsay et al., 2015; Marchitto et al., 2007), and Arabian Sea (Bryant et al., 2010). It has been hypothesized that these extremely ^{14}C-depleted waters are due to a breakdown in deep ocean stratification at the beginning of the deglaciation, and the subsequent transfer of a ^{14}C-depleted water mass to intermediate waters, particularly to Subantarctic Mode Water (SAMW) and Antarctic Intermediate Water (AAIW) as seen in ^{13}C records of planktonic foraminifera (Spero & Lea, 2002). However, evidence of this mechanism closer to the formation areas of intermediate and deep waters has not been found (e.g., Burke & Robinson, 2012; De Pol-Holz et al., 2010; Rose et al., 2010). An alternative hypothesis suggests that the extremely ^{14}C-depleted deepwater records of the SWP and EPR (Ronge et al., 2016) stem from enhanced local ^{14}C-dead CO_2 production in oceanic ridges during glacial periods. This hypothesis is supported by independent evidence of enhanced undersea volcanism during the last deglacial period, driven by lower sea level and reduced pressure in the deep ocean (Crowley et al., 2015; Lund & Asimow, 2011; Tolstoy, 2015).

While it is important to identify the mechanisms leading to the formation of the glacial deep ocean carbon reservoir, it is equally important to understand the mechanisms associated with its release to the atmosphere. During the last deglaciation, the SO and the EEP registered changes suggesting that both areas had a key role in the ventilation of the CO_2-rich/^{14}C-depleted deep ocean reservoir. Carbon isotope and opal flux records reveal sustained conditions of increased upwelling and/or decreased stratification between the upper and deep oceanic circulation cells in the SO during the deglaciation, diminishing only during the Antarctic Cold Reversal (ACR; Anderson et al., 2009; Siani et al., 2013). At the same time, boron isotope records suggest enhanced outgassing of CO_2 in both the SO and EEP during the deglaciation (Martínez-Botí et al., 2015). In addition, tephrochronology records indicate high ^{14}C Surface Reservoir ages (R_S) in the SO at the beginning of the deglaciation, suggesting upwelling of ^{14}C-depleted water to the surface (Siani et al., 2013; Sikes & Guilderson, 2016; Sikes et al., 2016; Sikes et al., 2000; Skinner et al., 2015). Meanwhile, in the Galapagos platform, R_S estimated by tuning between different records (Bova et al., 2018; De la Fuente et al., 2015; Umling & Thunell, 2017) yield R_S even higher than in the SO. In contrast, the EEP region along the south American margin, the R_S obtained by tuning (Bova et al., 2018) and by wood-planktic foraminifera pairs (Zhao & Keigwin, 2018) yield generally lower values. In conclusion, the exact mechanism(s) of carbon release remains highly debated, and more work is still needed to understand the details of oceanic circulation changes, from the LGM into the Holocene, that control this ventilation.

The Southeast Pacific (SEP) is a key region for testing these hypotheses since it is influenced by water masses originating in the SO, the EEP, and the NP (Figure 1). Our studied area therefore captures the different signals propagating from each of these regions, potentially allowing us to distinguish the local processes occurring in the SO and EEP from those in the NP. So far only two cores have been studied in the SEP using ^{14}C to interpret ventilation changes (Figure 1): core SO161-22SL (from now on 22SL, ~1,000 m, ~36°S; De Pol-Holz et al., 2010) and core MD07-3088 (~1,500 m, ~46°S; Siani et al., 2013). Based on carbon isotope data and tephrochronology estimates of R_S, Siani et al. (2013) inferred enhanced upwelling in the Pacific area of the SO during the last deglaciation and found ^{14}C-depleted waters during the LGM (~350‰ $\Delta^{14}C$ lower than the contemporary atmosphere) in line with a large number of deep cores in the Pacific Ocean (De la Fuente et al., 2015; Galbraith et al., 2007; Keigwin & Lehman, 2015; Rae et al., 2014; Ronge et al., 2016; Sikes et al., 2016; Skinner et al., 2015; Umling & Thunell, 2017).

These two locations capture only a narrow depth range (Figure 1), which could have missed the core of intermediate waters and potentially the ^{14}C-depleted deepwater reservoir. In order to obtain a more complete picture of the ventilation history in the SEP during the last deglaciation, we here report ^{14}C ages of planktic and benthic foraminifera and stable isotope ($\delta^{13}C$) measurements in planktic foraminifera, from

10.1029/2019PA003613

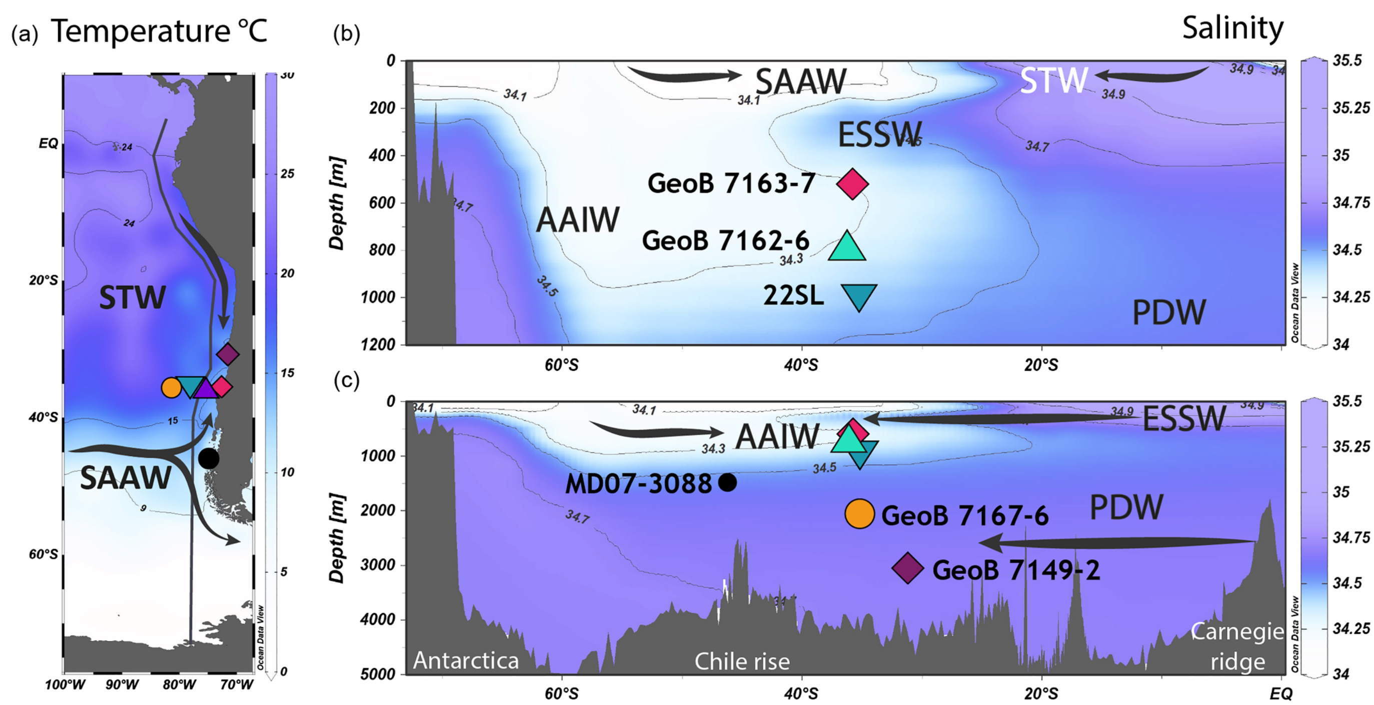

Figure 1. (a) Position of the studied cores (Table S3) and core MD07-3088 (Siani et al., 2013) in a sea surface temperature map. Also presented are the surface water masses in the area: Subantarctic Water (SAAW), transported by the Antarctic Circumpolar Current, and Subtropical Water (STW), transported by the Perú-Chile Countercurrent; (b) main water masses discussed in the text indicated by the salinity distribution obtained from gridded WOCE data (Gouretski & Koltermann, 2004) along the transect shown in gray in (a) in depths from 0 to 1,200 m; (c) same as (b) but between 0- and 5,000m depth. Visualization is based on Ocean Data View (Schlitzer, 2018). All studied core sites are indicated by the respective colored symbols. AAIW = Antarctic Intermediate Water; ESSW = Equatorial Subsurface Water; PDW = Pacific Deep Water.

five sediment cores, including new ^{14}C ages for core 22SL. This new set of marine sediment cores spans from ~31°S to 36°S and ~540 to 3,100 m water depth along the Chilean continental margin (Figure 1), providing a more complete perspective of ventilation and water mass changes during glacial-interglacial cycles.

2. Oceanographic Setting

The SEP is influenced by water masses originating in the SO, the EEP, and the NP (Figure 1). Subantarctic Water (SAAW), SAMW, and AAIW form in the SO; Equatorial Subsurface Water (ESSW) in the EEP; and Pacific Deep Water (PDW) originates in the NP and North Atlantic, primarily. SAAW is found along the Chilean margin from ~52°S to ~28°S (Silva et al., 2009) from the surface to ~100 m depth. It originates from upwelled water in the Antarctic divergence zone (Tomczak & Godfrey, 2003) and is advected by the Antarctic Circumpolar Current (ACC) until it encounters the American continent between ~42°S and 48°S where it divides in two branches, the southward flowing Cape Horn Current and the northward flowing Peru-Chile Current or Humboldt Current (Silva & Neshyba, 1977, 1980; Strub et al., 1998). Northward of ~28°S, the surface layer is occupied by Subtropical Water (STW), advected southward by the Peru-Chile Countercurrent (PCCC, Strub et al., 1998).

Underneath surface waters, the ESSW is transported from the EEP to the south (Figure 1) by the Peru-Chile Undercurrent along the Chilean margin (Silva et al., 2009; Silva & Fonseca, 1983; Strub et al., 1998; Wooster & Gilmartin, 1961; Wyrtki, 1967) and at ~80°W by the PCCC (Silva et al., 2009). Its core is characterized by a subsurface salinity maximum at ~250 m depth (Figure 1), which can still be identified at ~48°S, though not further than ~100 km from the coast (Silva et al., 2009). The ESSW is also characterized by low oxygen content, derived from the advection of waters from the Oxygen Minimum Zone of the EEP.

Information on ^{14}C content in the water column for the region is scarce. The most detailed record is station P06-E11 (~32.5°S) from the World Ocean Circulation Experiment-Hydrographic Program (Kumamoto et al., 2011).

10.1029/2019PA003613

Because of the "bomb effect," which doubled the ^{14}C content of the atmosphere in the 1950s and 1960s, the amounts of ^{14}C have been modified from the surface down to ~1,500 m in the SEP. However, prebomb $\Delta^{14}C$ values has been estimated from silicate concentrations, alkalinity, and apparent oxygen utilization by Kumamoto et al. (2011), which is here used as reference for depths shallower than 1,500 m (Figure S2 in the supporting information).

SAMW and AAIW originate in the SO and, in the SEP, have very similar characteristics (McCartney, 1977). In particular, AAIW ventilates intermediate waters from ~400 to 1,000 m depth with its core at ~600 m (Silva et al., 2009), easily identified as a salinity minimum (Figure 1; Johnson, 1973; Reid, 1965; Tsuchiya & Talley, 1996, 1998). Both SAMW and AAIW presently form in various areas of the SO, where recently upwelled deep waters subduct into intermediate depths ventilating the thermocline in the Pacific, Atlantic, and Indian oceans (Bostock et al., 2013; McCartney, 1977; Piola & Gordon, 1989). The exact subduction and formation mechanisms of these water masses are still debated (see Bostock et al., 2013, for a more detailed discussion on AAIW formation and Sloyan et al., 2010, for SAMW and AAIW). The SEP has been indicated as the main modern source of AAIW (e.g., Bostock et al., 2013; McCartney, 1977, 1982; Talley, 1996, 1999); from there it circulates to the north to enter the south Pacific subtropical gyre circulation and to the east through the Drake Passage into the Atlantic Ocean (Talley, 2013; Tomczak & Godfrey, 2003). The prebomb $\Delta^{14}C$ estimate for the depths bathed by AAIW in the SEP ranges between approximately −150‰ and approximately −100‰ $\Delta^{14}C$ (Figure S2).

Off Chile, at depths deeper than ~1,200 m, the PDW circulates to the south (Silva et al., 2009). PDW is the most ^{14}C-depleted water mass in the modern ocean, with $\Delta^{14}C$ values in the SEP between approximately −150‰ and −230‰ $\Delta^{14}C$ (Kumamoto et al., 2011). The formation of PDW is associated with sluggish mixing processes between Antarctic Bottom Water (AABW), AAIW, and recirculated North Atlantic Deep Water (NADW) along their way to the north Pacific (Talley, 2013; Tomczak & Godfrey, 2003); from there PDW circulates back south and is recognized by low ^{14}C and high nutrient contents.

3. Materials and Methods

Marine sediment cores GeoB 7167-6, GeoB 7163-7, GeoB 7162-6, GeoB 7149-2, and 22SL (Figure 1) were retrieved by the German r/v Sonne during expeditions SONNE 156 (Hebbeln and cruise participants, 2001) and SONNE 161 (Wiedicke-Hombach et al., 2002). Cores GeoB 7167-6, GeoB 7163-7, GeoB 7162-6, and 22SL were obtained at ~36°S, off Concepción, where sedimentation rates are very high (~40 cm/kyr) due to high terrestrial input derived from rivers (Hebbeln et al., 2007). Core GeoB 7149-2 was recovered at ~31°S off Puerto Oscuro. Despite being adjacent to the semidesert areas of the "Norte Chico," sedimentation rates at GeoB 7149-2 are relatively high, varying between 20 and 40 cm/kyr due to quasi-perennial upwelling-driven marine productivity (De Pol-Holz et al., 2007).

The planktic foraminifera species—*N. dutertrei*, *N. pachyderma* (syn) (i.e., *N. pachyderma*), *N. pachyderma* (dex) (i.e., *N. incompta*), *G. bulloides*, and *G. inflata*—and the benthic foraminifera species—*Uvigerina sp.* and *Brizalina sp.*—were handpicked for monospecific dating when possible. Otherwise, mixed planktic foraminifera (*N. pachyderma* (syn), *N. pachyderma* (dex), *N. dutertrei*, and *G. bulloides*) and mixed benthic foraminifera (*Uvigerina sp.*, *Bolivina sp.*, *Angulogerina sp.*, *Globocassidulina sp.*, and *Dentalina sp.*) were measured. Foraminifer abundances limited the time span and resolution of some of the ^{14}C and ^{13}C records. Detailed information on each sample is provided in Table S1. All ^{14}C measurements were carried out at the Keck Carbon Cycle Accelerator Mass Spectrometer facility at the University of California, Irvine, except for published data from core 22SL (De Pol-Holz et al., 2010), dated at the National Ocean Science Accelerator Mass Spectrometer facility at the Woods Hole Oceanographic Institution. Briefly, samples were leached by 10% of their mass using HCl in order to remove any secondary (younger) carbonate and then hydrolyzed with 85% H_3PO_4 under vacuum. Finally, all samples were graphitized using Fe as a catalyst in the presence of H_2. All ^{14}C dates are shown in Table S1 and plotted in Figure S1.

Stable isotopes of carbon ($\delta^{13}C$) were obtained for the planktic foraminifera *Globigerina bulloides* every 5 cm, where possible, in the size range >212 μm, in cores GeoB 7163-6, GeoB 7167-6, 22SL, and GeoB 7149-2. Additionaly, *N. dutertrei* was measured in core GeoB 7149-2. Analyses were performed at the MARUM Stable Isotope Laboratory on a Thermo Finnigan MAT 252 mass spectrometer linked online to a

CarboKiel-II carbonate preparation device. Long-term standard deviation was monitored through the internal laboratory standard Solnhofen Limestone (SHK) with errors estimated in 0.05‰ V-PDB for $\delta^{13}C$. Isotope values were calibrated to the Vienna Pee dee Belemnite scale with the NBS-19 standard. Results are presented in Table S2.

4. Age Models

Correcting planktic foraminifera ^{14}C ages for a constant R_S has been broadly utilized as a method to produce marine sediment core chronologies (e.g., De Pol-Holz et al., 2010; Kaiser et al., 2008; Lamy et al., 2004). However, the assessment of precise R_S has demonstrated that these can vary greatly during the Holocene (Carré et al., 2015; Latorre et al., 2017) but especially during the late glacial and last deglaciation (Siani et al., 2013; Sikes & Guilderson, 2016; Sikes et al., 2000; Sikes et al., 2016; Skinner et al., 2015). In particular, Siani et al. (2013) demonstrated the varying nature of the R_S in the SEP between ~15 and 2 ka cal BP, using tephrochronology in core MD07-3088 (~46°S) and obtaining R_S values ranging between 790 ± 160 years and 1,320 ± 95 years. In order to obtain robust chronologies, we assess R_S changes at ~36°S and ~31°S since the LGM.

In the modern SEP, R_S ages result from a combination of SAAW or STW (Figure 1) with relatively ^{14}C-depleted ESSW (Figure S2), which is brought to the surface by coastal upwelling (Strub et al., 1998). Broadly, three different coastal upwelling regimes exist, which are controlled by the position of the Southerly Westerly Winds (SWW): (i) south of ~39°S, the permanent presence of SWW inhibits upwelling; thus, R_S there are controlled mainly by the presence of SAAW; (ii) between ~35°S and 39°S, coastal upwelling is seasonal, because of the latitudinal shift of the SWW to the south in Austral summer allowing coastal upwelling to occur; (iii) north of ~35°S, coastal upwelling is permanent, and the highest R_S are found in this area (Carré et al., 201; Ingram & Southon, 1996; Merino-Campos et al., 2019; Ortlieb et al., 2011; Taylor & Berger, 1967). These different domains of upwelling can also be observed in $\delta^{13}C$ measurements in planktic foraminifera in the modern SEP. At present, *G. bulloides* is interpreted to live in the surface mixed layer and prefer upwelling conditions, in the SEP (Marchant et al., 1998) and elsewhere (Bemis et al., 1998; Fairbanks et al., 1982; Ortiz et al., 1995; Sautter & Thunell, 1991). On the other hand, *N. pachyderma* (dex) has been suggested to prefer a more stratified surface layer (Marchant et al., 1998; Mortyn & Charles, 2003; Ortiz et al., 1995, 1996; Sautter & Thunell, 1991). Between ~39°S and 46°S, both species yield similar values (Figure S2), consistent with a lack of upwelling, whereas between ~24°S and 35°S, $\delta^{13}C$ values of *G. bulloides* are ~1.5‰ lighter than *N. pachyderma* (dex), consistent with persisting upwelling conditions in this area (Mohtadi et al., 2005). As a result, $\delta^{13}C$ records of *G. bulloides* are expected to reflect differences in R_S at ~46°S, ~36°S, and ~31°S resulting from differing contributions of SAAW and ESSW due to variations in the intensity of coastal upwelling along the margin. Additionally, R_S variations in the past may have occurred because of changes in the ^{14}C signature of the upwelled waters and/or because of modifications in habitat preferences of planktonic foraminifera.

To assess the relative contribution of SAAW to R_S at ~36°S and ~31°S in the past, we compare the *G. bulloides* $\delta^{13}C$ records of this study versus core MD07-3088 at ~46°S. *G. bulloides* $\delta^{13}C$ in core MD07-3088 is interpreted to represent the SAAW end member because of its position directly influenced by the ACC and no coastal upwelling (Strub et al., 1998). In order to assess how R_S varies with latitude, the $\delta^{13}C$ records are plotted against their planktic conventional ^{14}C ages (Figure 2). Similar trends are observed at ~36°S and ~46°S (Figure 2d), with a distinct "W"-shaped trend in both latitudes but not at ~31°S. However, from ~15 ^{14}C ka BP, $\delta^{13}C$ values of *G. bulloides* at ~36°S become relatively lower than at ~46°S, similar to what is observed today (Figure S2). In addition, between ~13 and 11 ^{14}C ka BP (gray interval in Figure 2), values at ~36°S appear to lag ~500–700 ^{14}C years behind the $\delta^{13}C$ of *G. bulloides* at ~46°S.

In the SEP, the deglaciation is characterized by abrupt changes in surface water properties that have been interpreted as a reorganization of water masses and fronts (e.g., Haddam et al., 2018; Kaiser et al., 2008; Mohtadi et al., 2008), associated with the meridional migration of the SWW to the south and/or changes in its distribution and intensity. The transition from higher to lower $\delta^{13}C$ at ~36°S (22SL) from ~16 to 14 ^{14}C ka BP (Figure 2d) is consistent with the migration of the SWW to the south at the beginning of the deglaciation (Denton et al., 2010; Mohtadi et al., 2008; Moreno et al., 1999) allowing the onset of seasonal

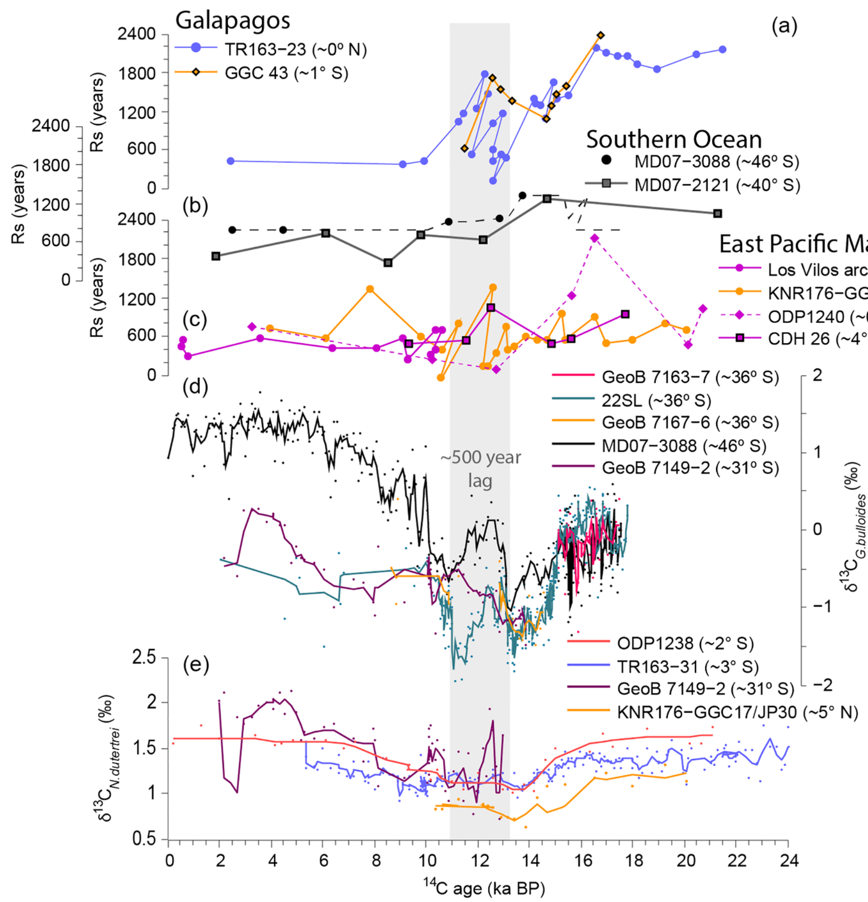

Figure 2. Comparison of records in the South East Pacific with records in the Southern Ocean and Equatorial East Pacific against ^{14}C age of planktic foraminifera, rather than calendar age. In order to do this, the ^{14}C dates were interpolated to obtain ^{14}C estimates for the depths in which only ^{13}C was measured. For depths where more than one planktic foraminifera specie was dated, the mean at each depth was used as references for the interpolation. R_S estimates in (a) Galapagos platform: core TR163-23 (0.41°S, 92.16°W, 2,730 m; Umling & Thunell, 2017), from tuning with Greenland Ice Core Chronology GICC05 and core GGC 43 (1°15.13′S, 89°41.07′S, 617 m; Bova et al., 2018); (b) the Southern Ocean, from tephrochronology in core MD07-3088 in the South East Pacific sector (41°S, 74°W, 1,536 m; Siani et al., 2013; symbols are the measured R_S while the black line corresponds to the interpolated values) and core MD97-2121 (40°22.935′S, 177°59.68′E, 2,314 m; Skinner et al., 2015) the South West Pacific sector; (c) the East Pacific margin, at ~32°S obtained from paired mollusk shells and charcoal fragments from archeological sites near Los Vilos (Carré et al., 2015); in core CDH 26 (3°59.16′S, 81°18.52′W, 1,023 m; Bova et al., 2018) from tuning with EPICA Dome C and in core KNR176-GGC17/JP30 (5.02°N, 77.63°W, 707 m; Zhao & Keigwin, 2018) from wood-planktic foraminifera pairs. (d) *G. bulloides* δ^{13}C from cores used in this study and core MD07-3088 (Siani et al., 2013), the lines correspond to smoothed 3-point moving averages of the original data (small symbols). (e) *N. dutertrei* δ^{13}C in the Equatorial East Pacific: core TR163-31 (3°37.2′S, 83°58′W, 3,210 m; Patrick & Thunell, 1997) and ODP site 1238 (1°52.2′S, 82°46.8′W, 2,203 m; Martínez-Botí et al., 2015) compared with *N. dutertrei* δ^{13}C GeoB 7149-2; the lines correspond to smoothed 3-point moving averages of the original data (small symbols). Gray interval: ~500 years lag between the δ^{13}C record at ~46°S and ~36°S discussed in the text.

upwelling at this latitude, thus establishing a situation similar to what is observed today (Figure S2). In addition, between ~13 and 11.5 ^{14}C ka BP not only does δ^{13}C become relatively more depleted but also radiocarbon dates of planktic foraminifera are consistently older at ~36°S than at ~46°S. These observations are consistent with upwelling of older ESSW at 36°S between ~13 and 11.5 ^{14}C ka.

To observe how the R_S of the ESSW endmember changed, we use a broad range of cores in the EEP either with R_S assessments or stable isotope records. These cores are thought to record changes in the Equatorial Undercurrent (EUC), which feeds the ESSW (Brink et al., 1983; Lukas, 1986; Toggweiler et al., 1991). The comparison is based in measurements done on the deep-dwelling planktic foraminifera *N. dutertrei*, as they are thought to represent the geochemistry of the EUC (Fairbanks et al., 1982; Spero & Lea, 2002). The

10.1029/2019PA003613

observed lag between ~13 and 11.5 ^{14}C ka BP (gray interval in Figure 2) implies R_S ages ~500–700 ^{14}C years older at ~36°S than at ~46°S under the assumption that the "W"-shaped trend in both $\delta^{13}C$ records should be contemporaneous. When compared with other EEP records, the SO shows, in general, lower Rs values (Figures 2a–2c). The higher R_S in the EEP is probably the result of the extremely ^{14}C-depleted intermediate waters observed in this area (Bova et al., 2018; Stott et al., 2009), which would be even older than contemporaneous deep waters upwelling in the SO (Figures 6 and S4).

Since there is a lot of uncertainty on how much these source areas influenced each of our sites, four age models, each assigning different R_S to planktic foraminifera ^{14}C ages were built for each core accounting for four possible scenarios: (a) Surface water from SAAW was advected north of 46°S reaching as far north as 31°S throughout the considered period, and thus, R_S values from core MD07-3088 are applied to all studied cores; (b) between ~13 and 11 ^{14}C ka BP the upwelling of ^{14}C-depleted ESSW increases the R_S at ~36°S (22SL, GeoB 7167–6, and GeoB 7162–6), and thus, equatorial R_S from core TR163-23 are assigned for this interval to cores at ~36°S; (c) no changes occur in R_S, and thus, constant values, equivalent to the modern mean in the closest latitude with available information (Merino-Campos et al., 2019), are assigned; (d) at ~31°S (Geob 7149-2) exclusively equatorial waters flow in the whole interval, and thus, for ages older than ~11 ka ^{14}C BP, R_S from core TR163–23 (~0°N) are assigned, and for ages younger, R_S ages from ~32°S are assigned (Carré et al., 2015). See Table S2 for a summary.

After assigning the relevant R_S to each planktic foraminifera ^{14}C age, the age models for each core were generated using the Bacon algorithm (Blaauw & Christen, 2011). We then calculated the $\Delta^{14}C$ of deep and intermediate waters following Adkins and Boyle's (1997) definition derived from Stuiver and Polach (1977),

$$\Delta^{14}C = \left(\frac{e^{-\frac{^{14}C\ age}{8,033}}}{e^{-\frac{cal\ age}{8,266}}} - 1 \right) 1,000‰,$$

for each age model. The resulting $\Delta^{14}C$ values are presented in Figure 3 with their respective 1σ and 2σ envelopes.

In addition, the simulated variation of $\Delta^{14}C$ at each depth was obtained by a modern circulation model constrained by observations of temperature, salinity, CFC-11, and prebomb $\Delta^{14}C$ (DeVries, 2014). The model takes into account variations in the atmospheric ^{14}C and CO_2 concentration using the gas exchange formulation of DeVries and Primeau (2010; their equations B.6 and B.7). This formulation states that the gas exchange piston velocity for $\Delta^{14}C$ is proportional to the ratio of atmospheric pCO_2 to surface ocean DIC. To a first approximation we assume a globally uniform surface ocean DIC that varies with pCO_2 according to a buffer factor of 10 (i.e., a 10% change in atmospheric pCO_2 translates to a 1% change in DIC) in a modern oceanic circulation scenario. This model simulation thus approximates the expected $\Delta^{14}C$ that would arise in a scenario of constant (modern) ocean circulation and gas exchange piston velocity matching the observed modern $\Delta^{14}C$ relatively well at the core locations (Figure 3). For the model calculations, we used atmospheric ^{14}C concentration from the IntCal13 curve (Reimer et al., 2013), and atmospheric pCO_2 from ice core reconstructions (Marcott et al., 2014; Monnin et al., 2001), and air-sea piston velocity from the OCMIP-2 protocol, reduced by 20% globally in light of recent estimates (Sweeney et al., 2007). Deviations from the modeled $\Delta^{14}C$ can be interpreted as arising from changes in ocean circulation, changes in air-sea gas exchange due to changes in wind speed or sea ice cover, or from neglected sources and/or sinks of ^{14}C such as inputs of ^{14}C-dead carbon from hydrothermal vents. The model displays a slight positive bias of ~25–30‰ relative to the modern core-top $\Delta^{14}C$ values, which is likely due to the simplifications of the air-sea gas exchange parameterization. This positive bias is corrected for when comparing the modeled and observed variations in $\Delta^{14}C$.

5. Results

With the exception of age models using constant R_S (age model *c*), there is general agreement between the different age models and derived $\Delta^{14}C$ values (Figures 3 and S3). These age models represent the different scenarios depicted in section 4 and the most likely R_S given our current knowledge of the area. For cores

10.1029/2019PA003613

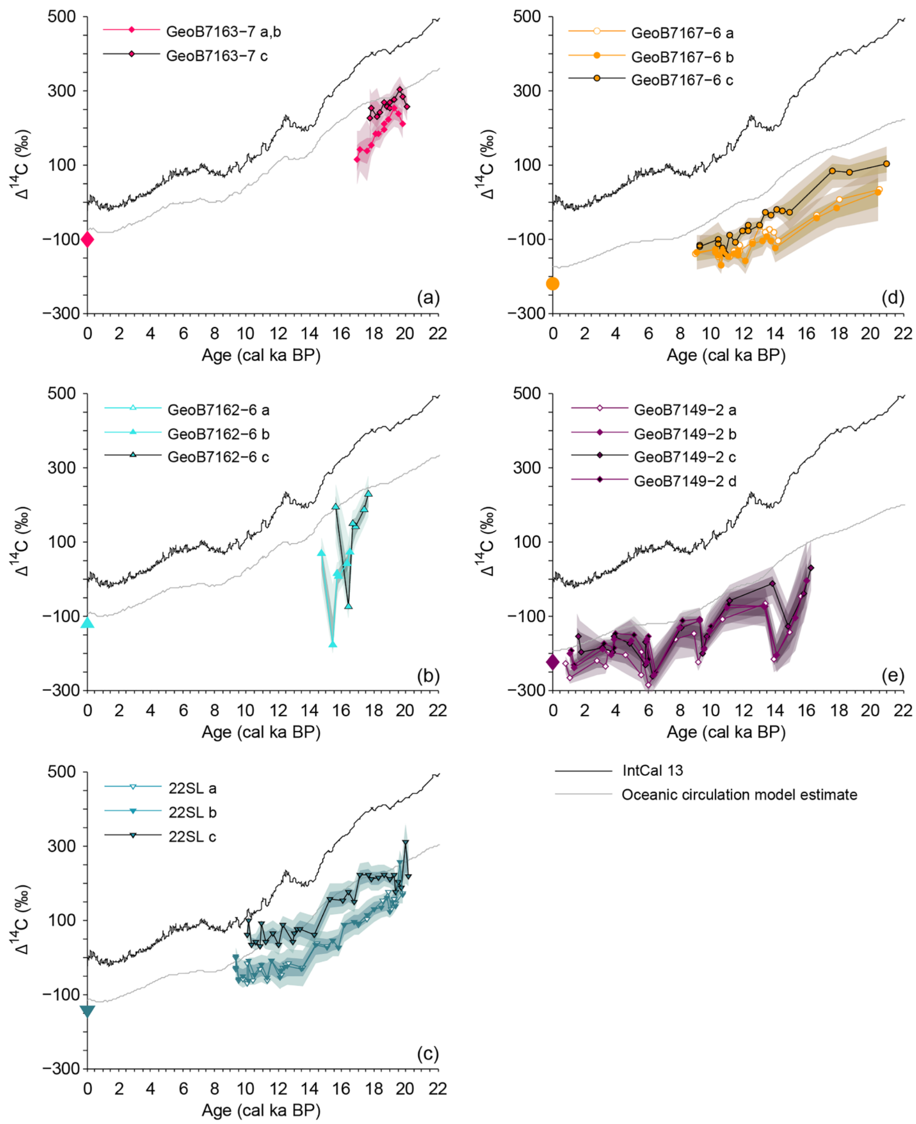

Figure 3. $\Delta^{14}C$ estimates for the cores in this study with their corresponding 1σ (dark) and 2σ (light) envelopes, which take into account errors in ^{14}C dating of benthic foraminifera and calendar ages estimates, from the different age model scenarios discussed in the text: (a) Surface water from SAAW was advected north of 46°S reaching as far north as 31°S throughout all the considered period, and thus, the R_S from core MD07-3088 are applied to all studied cores; (b) between ~13 and ~11 ^{14}C ka BP, the upwelling of ^{14}C-depleted ESSW increases the R_S at ~36°S (22SL, GeoB 7167–6, GeoB 7162–6), and thus, equatorial R_S from core TR163-23 are assigned for this interval to cores at ~36°S; (c) no changes occur in R_S, and thus, constant values, equivalent to the modern mean in the closest latitude with available information (Merino-Campos et al., 2019), are assigned; (d) at ~31°S (Geob 7149-2) exclusively equatorial waters flow in the whole interval, and thus, for ages older than ~11 ka ^{14}C BP, R_S from core TR163–23 (~0°N) are assigned, and for ages younger, R_S ages from ~32°S are assigned (Carré et al., 2015). Also plotted are the atmospheric $\Delta^{14}C$ (black line, Reimer et al., 2013), the modeled $\Delta^{14}C$ at each depth accounting for changes in atmospheric $\Delta^{14}C$ and CO_2 (gray curves), and the modern $\Delta^{14}C$ from station P06-E11 (Kumamoto et al., 2011).

at ~36°S, age models *a* and *b* yield virtually identical results, and the discussion is based on age model *b*, which takes into account a lag observed in the $\delta^{13}C$ records between ~36°S and ~46°S (Figure 2). Core GeoB 7149-2 presents more variability among the different age models during the Holocene. However, as described in section 4, R_S ages at ~31°S are probably lower than those for core MD07-3088, in agreement with values estimated at ~32°S (Carré et al., 2015). Consequently, the discussion for core GeoB 7149-2 is based on the results obtained with age model *d*.

10.1029/2019PA003613

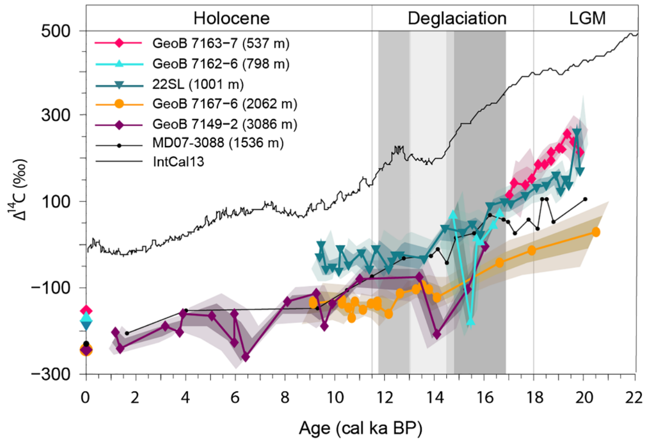

Figure 4. $\Delta^{14}C$ variations in intermediate and deep waters in the South East Pacific since the Last Glacial Maximum, from cores in this study with their corresponding 1σ (dark) and 2σ (light) envelopes, which take into account errors in ^{14}C dating of benthic foraminifera and calendar ages estimates. Also plotted are core MD07-3088, in the South East Pacific sector of the Southern Ocean (Siani et al., 2013), the atmospheric $\Delta^{14}C$ variation IntCal13 (black line, Reimer et al., 2013), and the modern $\Delta^{14}C$ estimate from station P06-E11 (~32°S) at each core depth (Kumamoto et al., 2011).

Additional information is provided by the modeled $\Delta^{14}C$ change at each depth (Figures 3 and 5), which is a reference on how the ^{14}C content of the water would change accounting only for changes in atmospheric pCO_2 and its ^{14}C content. The modeled $\Delta^{14}C$ is in general agreement with the modern data, with values ~20–30‰ $\Delta^{14}C$ higher than the modern in all cores except from GeoB 7167-6, which presents a difference of ~50 ‰ $\Delta^{14}C$ (Figure 3). In order to better visualize how much of the obtained $\Delta^{14}C$ in each core would not be accounted by changes in atmospheric pCO_2 and its ^{14}C content, the difference between the $\Delta^{14}C$ obtained with the selected age models and the modeled $\Delta^{14}C$ is also presented (Figure 5), corrected by the difference between the modern modeled value and the modern value (Figure S2). In Figure 5, a deviation from zero implies changes in oceanic circulation, in air-sea gas exchange (unrelated to pCO_2 changes, which are already accounted for in the model) and/or geologic input of ^{14}C-dead CO_2. Also, similar deviations from zero at the different analyzed depths imply that the relative amount of ^{14}C between them was similar to the modern.

During the LGM, $\Delta^{14}C$ records from all cores in the SEP are more depleted in ^{14}C with respect to the contemporaneous atmosphere than they are in the Holocene (Figure 4). The observed minus modeled $\Delta^{14}C$ is predominantly negative during the LGM (Figure 5), suggesting that the depleted ^{14}C values result from slower ventilation or older reservoir ages, rather than from changes in atmospheric ^{14}C or pCO_2. The variation of ^{14}C with depth is similar to the modern ocean above ~1,500 m (Figures 4 and 5) suggesting similar water column structures during the LGM and early Holocene (Figure 4), though with slightly more ventilated waters at ~540 m. Meanwhile, at ~2,000 m the only available data point is the most depleted both compared with the atmosphere and the modeled values, in agreement with a broad range of deepwater records (Figure 7). Unfortunately, there are no contemporaneous data points at ~1,500 and ~2,000 m for the glacial in the SEP; however, we can at least obtain the difference between the mean values at each depth, which is ~66‰ $\Delta^{14}C$ (Figure 4) whereas the modern difference is ~20‰ $\Delta^{14}C$. This difference also stands when comparing with the simulated $\Delta^{14}C$ values at each depth (Figure 5a), where waters at ~2,000 m are ~25‰ more depleted with respect to the simulated estimated than at ~1,500 m. The above information suggests a more ^{14}C-depleted and stratified deep glacial ocean, in particular below ~1,500 m.

Between ~19 and 17 ka cal BP, the $\Delta^{14}C$ signature of waters at ~1,000, ~1,500, and ~2,000 m maintains a stable offset from the modeled estimate (Figure 5). At ~540 m, however, $\Delta^{14}C$ values become rapidly more ^{14}C depleted at ~19 ka cal BP, decreasing from a mean difference with waters at ~1,000 m of ~54‰ $\Delta^{14}C$ in the LGM to ~29‰ $\Delta^{14}C$ in the early deglaciation (~17 ka; Figure 4). Between ~16.5 and 14.8 ka cal BP, intermediate waters at ~800 and ~1,000 m become more ^{14}C depleted with respect to the atmosphere and model; meanwhile, waters at ~1,500 m become more ventilated, reaching similar values to those found at ~800 and ~1,000 m until ~14.8 ka cal BP (Figure 4). At ~800 m, waters reach an extremely ^{14}C depleted minimum of ~460‰ $\Delta^{14}C$ lower than the contemporary atmosphere and ~350‰ $\Delta^{14}C$ lower than the modeled estimate. Between ~18 ka cal BP and ~14 ka cal BP, the only data point available at deep waters at ~2,000 m remains as ^{14}C depleted from the model as during the LGM (Figure 5), with a difference from the contemporary atmosphere of approximately −380‰ $\Delta\Delta^{14}C$. At ~3,000 m, values are both more ^{14}C enriched (~16 ka cal BP) and more 14C depleted (~14 ka cal BP) than at ~2,000 m, and a decreasing trend is observed between ~16 and 14 ka cal BP, reaching a minimum of approximately −400‰ $\Delta\Delta^{14}C$ at ~14 ka cal BP.

Around ~14.5 ka cal BP, benthic foraminifer $\Delta^{14}C$ offsets from the model measured at water depths between 1,000 and 3,000 m briefly return to LGM values; waters at ~1,500 m are more poorly ventilated (larger offset), while waters at ~800 and ~1,000 m are better ventilated (smaller offsets). Between ~13.5 and 10.5 ka cal BP intermediate waters at ~1,000 and 1,500 m return to a situation similar to what is observe between ~16.5 and ~14.5 ka cal BP, whereas deep waters at ~2,000 and ~3,000 m become rapidly ventilated at ~13 ka cal BP. In particular, waters at ~2,000 m go from a $\Delta\Delta\,^{14}C$ of −320‰ at ~14 ka cal BP to −280‰ at ~13.5 ka cal BP and at ~3,000 m from −400‰ $\Delta\Delta\,^{14}C$ at ~14 ka cal BP to −270 at ~13.3 ka cal BP. Between ~13.5 and 12.5 ka cal

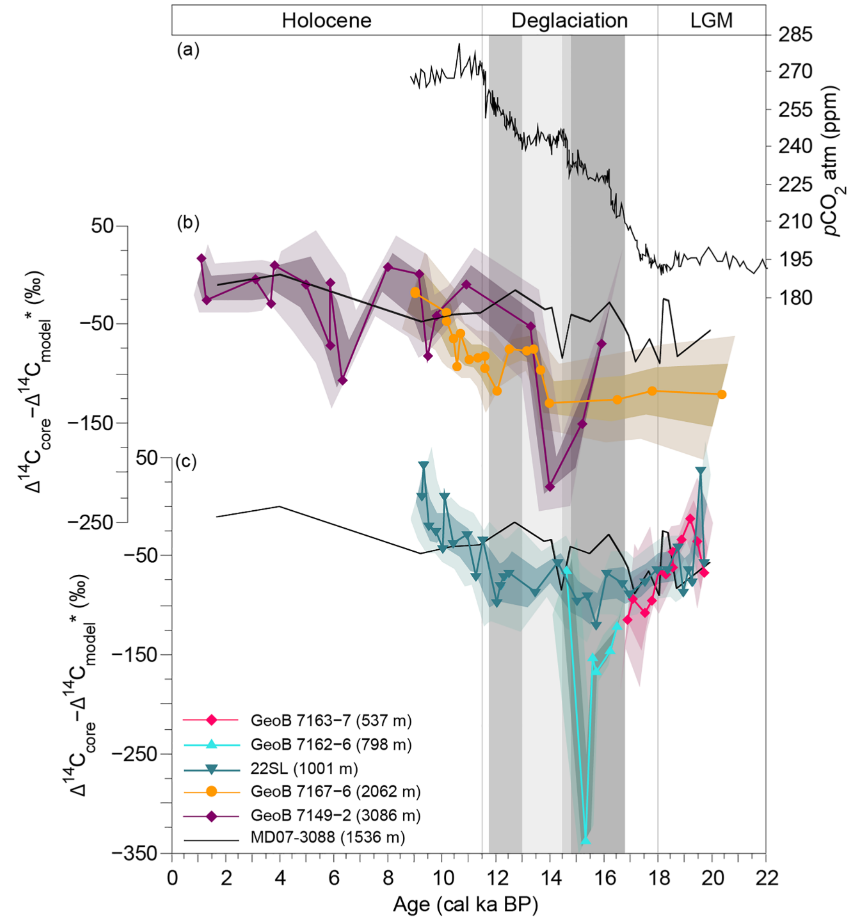

Figure 5. (a) Atmospheric pCO_2 from West Antarctic Ice Sheet Divide ice core (Marcott et al., 2014). (b) Deviation of the obtained $\Delta^{14}C$, in cores in the South East Pacific, from the modeled estimate, corrected by the difference between the modern modeled estimate and the modern natural $\Delta^{14}C$ at each depth (Kumamoto et al., 2011). Also plotted are their corresponding 1σ (dark) and 2σ (light) envelopes, which take into account errors in ^{14}C dating of benthic foraminifera and calendar ages estimates and the error associated with the model.

BP, waters at ~2,000 m stay relatively well ventilated and at ~12.1 ka cal BP decrease its $\Delta\Delta\,^{14}C$ in about 40‰; from there they become increasingly better ventilated until the end of the record around 9 ka cal BP. At ~10 ka cal BP, all records with available information reach values similar to modern, and the difference with the modeled estimates is close to zero.

6. Discussion

6.1. Last Glacial Maximum

The obtained $\Delta^{14}C$ data at ~2,000 m show a depletion from the contemporary atmosphere of approximately −410‰ (Figure 4), which agrees with a broad range of other deepwater records (Figure 6): approximately −310‰ to −600‰ in the SWP (Ronge et al., 2016; Sikes et al., 2016), approximately −400‰ to −540‰ in the SA (Skinner et al., 2010), approximately −370‰ to −500‰ in the NP (Galbraith et al., 2007; Rae et al., 2014), and approximately −400‰ to −480‰ in the EEP (De la Fuente et al., 2015; Umling & Thunell, 2017). These glacial deep ocean values show relatively larger depletion than modern data but not as extremely ^{14}C-depleted values as observed in the SWP and EPR, where ^{14}C contents were between approximately −900‰ to −1,000‰ lower than the contemporary atmosphere (Ronge et al., 2016). Therefore, the new SEP ^{14}C data contribute to the idea that the widespread situation during the LGM was a relatively ^{14}C-depleted deep ocean with only localized extreme depletions. Above these depths, at ~1,500 m, values are ~66‰ $\Delta^{14}C$ higher than the point at ~2,000 m, a difference three times higher than

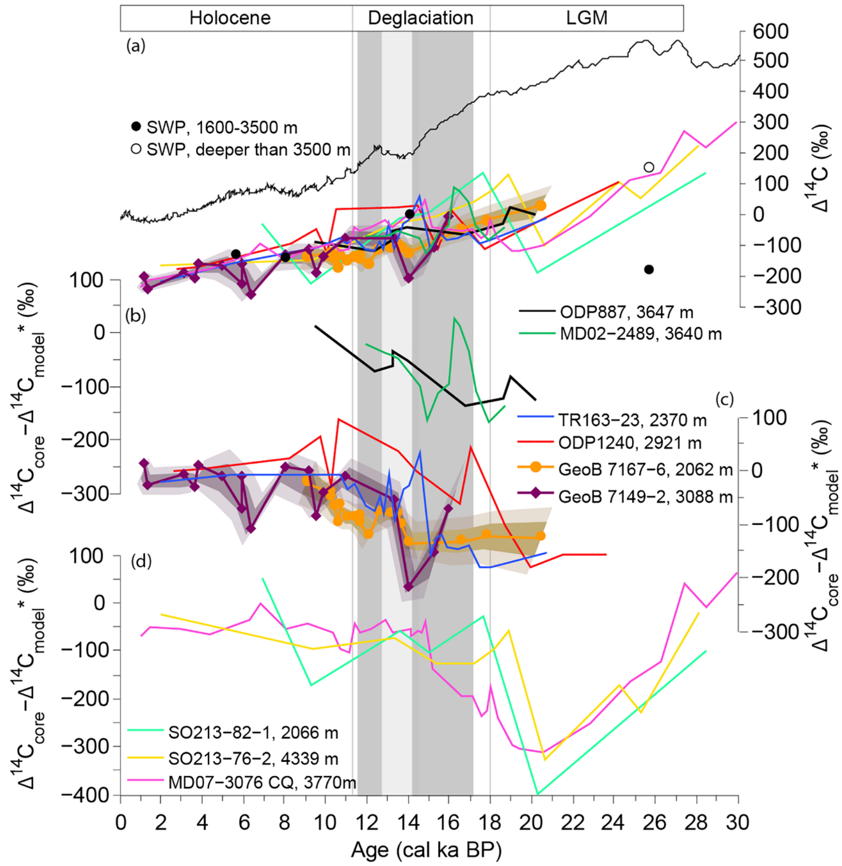

Figure 6. (a) $\Delta^{14}C$ variations in deep waters in the Pacific Ocean and South Atlantic along with the atmospheric $\Delta^{14}C$ variation IntCal13 (black line; Reimer et al., 2013). South West Pacific mean values at depths between 1,600–3,500 m and deeper than 3,500 m (Sikes et al., 2016) together with cores described in (b), (c), and (d), which correspond to the deviation of the $\Delta^{14}C$ in deep waters from the modeled estimate, corrected by the difference between the modern modeled estimate and the modern $\Delta^{14}C$ at each depth from GLODAPv2 (Key et al., 2015). (b) North Pacific: ODP887 (54.4°N, 148.5°W, 3,647 m; Galbraith et al., 2007), MD02-2489 (54.4°N, 149°W, 3,640 m, Rae et al., 2014); (c) Equatorial East Pacific: ODP1240 (0°N, 86.5°W, 2,921 m; De la Fuente et al., 2015), TR163-23 (0.4°N, 92.2°W, 2,730 m; Umling & Thunell, 2017), and South East Pacific records GeoB 7167-6 and GeoB 7149-2 from this study. (d) South West Pacific (Ronge et al., 2016): SO213-82-1 (45.8°S, 176.6°E), PS75/100-4 (45.8°S, 177.1°E, 2,498 m); SO213-76-2 (46.2°S, 178°E, 4,339 m), and South Atlantic (Skinner et al., 2010): MD07-3076 CQ (44°4.46′S, 14°12.47′W, 3,770 m).

modern (Figure 4). In contrast, the relative $\Delta^{14}C$ values at ~540, ~1,000, and ~1,500 m suggest a glacial structure similar to the modern ocean (Figure 4), though with relatively more ventilated waters at ~540 m.

The observed structure is consistent with the idea of a more stratified deep glacial ocean (e.g., Burke & Robinson, 2012; Ronge et al., 2016; Sikes et al., 2017) in which less ventilated deep waters and increased carbon storage were associated to a stronger geochemical divide between middepth and deep waters (Toggweiler, 1999). Different hypotheses have been called upon to explain the observed changes in the glacial ocean (Adkins, 2013; Ferrari et al., 2014; Keeling & Stephens, 2001; Watson & Naveira Garabato, 2006). These hypotheses have in common the importance of sea ice extension, controlling gas exchange between deep waters and the atmosphere (Ferrari et al., 2014; Stephens & Keeling, 2000) and/or by modulating the production and density of deep SO waters (Adkins, 2013; Keeling & Stephens, 2001; Watson & Naveira Garabato, 2006). During the late glacial, freshening of surface waters in the SO would be diminished by the presence of more extensive sea ice, blocking precipitation (Keeling & Stephens, 2001), and/or decreasing sea ice melt water supply (Adkins, 2013; Keeling & Stephens, 2001). This, together with a colder water column, would result in production of denser deep waters in the SO (Adkins, 2013; Watson & Naveira Garabato, 2006), where density would be salt, rather than temperature controlled, as observed in pore water chloride (Adkins et al., 2002). This would decrease isopycnal mixing between southern sourced deep waters

10.1029/2019PA003613

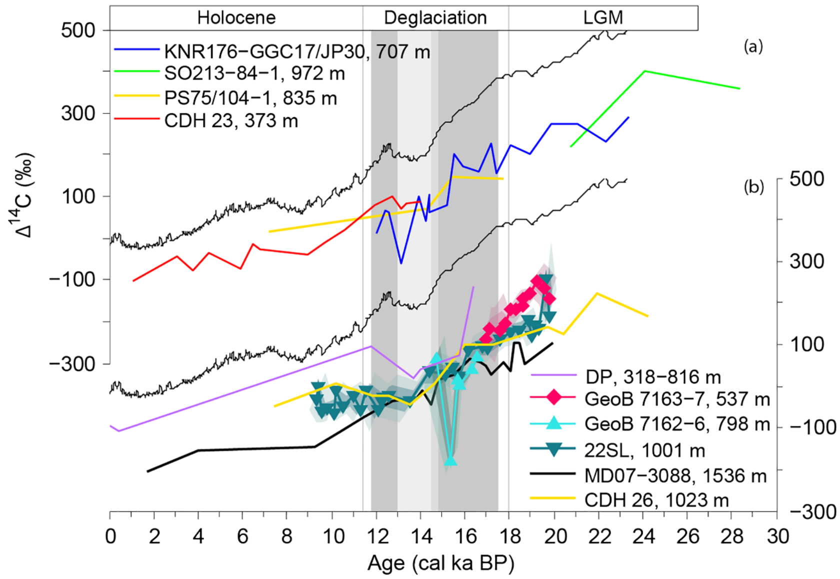

Figure 7. $\Delta^{14}C$ variations in intermediate waters in the Pacific Ocean and Drake Passage along with the atmospheric $\Delta^{14}C$ variation IntCal13 (black line, Reimer et al., 2013). (a) Records where no decreased ventilation is observed during the deglaciation: KNR176-GGC17/JP30 (5.02°N, 77.63°W; Zhao & Keigwin, 2018); SO213-84-1 (45°123′S; 174°58′E; Ronge et al., 2016); PS75/104-1 (44°77′S, 174°52′E; Ronge et al., 2016); CDH 23 (3°44 to 95′S, 81°08.05′W; Bova et al., 2018). (b) Records interpreted as deeper convection of the AAIW during the deglaciation, as indicated in the text: Corals in the Drake Passage (DP) between 318 and 816 m (Burdwood Bank; Burke & Robinson, 2012); MD07-3088 (46°S, 75°W; Siani et al., 2013); CDH 26 (3°59.16′S, 81°18.52′W; Bova et al., 2018).

and NADW, a mechanism that today helps ventilate the deep ocean (Adkins, 2013). Additionally, Ferrari et al. (2014) proposed that the depth of the waters upwelling in the SO would be controlled by the latitude at which the Antarctic divergence occurs, given by the zero-buoyancy boundary. This, in turn would be bounded to the quasi permanent sea ice extent (Ferrari et al., 2014), which is thought to have extended north during the LGM (Gersonde et al., 2005; Otto-Bliesner et al., 2007). When the zero buoyancy boundary moves northward along with sea ice, deep waters that were previously upwelling north of it, thus forming intermediate waters, upwell south of it, forming deep and abyssal deep waters instead. This would enhance carbon and nutrient trapping in the Southern Ocean (Primeau et al., 2013; Holzer et al., 2014), further contributing to a buildup of respired carbon in an isolated Southern-sourced water mass in the deep ocean. Ferrari et al. (2014) estimate that a northern extent of the quasi permanent sea ice would shoal the depth of the isopycnes upwelling in the divergence zone by ~500 m, consistent with findings in the Atlantic and Pacific Oceans (e.g., Sikes et al., 2017). This would have a double effect in the ventilation of the deep ocean. On the one hand, a larger proportion of the deep ocean would upwell south of the zero-buoyancy boundary under quasi permanent sea ice, where the extent of gas exchange with the atmosphere is decreased (Stephens & Keeling, 2000). On the other hand, the shoaling of the upwelled waters would additionally act to diminish the ventilation of abyssal waters since topography-driven turbulent mixing across isopycnals is higher below the reach of seamounts and mid-ocean ridges, near ~2,000-m depth (Figure 1; Adkins, 2013; Ferrari et al., 2014) and waters below this depth would upwell to the south of the divergence zone during the LGM. Additionally, it has been suggested that a northern position of the SWW during the glacial would result in less upwelling of warmer waters, reinforcing the development of the sea ice, thus working together with the previously described processes to develop the isolated deepwater reservoir (Toggweiler et al., 2006).

The high contrast in ^{14}C content of waters at ~1,000, ~1,500, and ~2,000 m observed in the SEP, much higher than today, with waters at ~2,000 m especially ^{14}C depleted, argues in favor of decreased mixing between waters above and below this depth. The latter would result from decreased ventilation of the deep ocean and a lesser contribution of deep waters in the formation of intermediate waters consisting with the aforementioned glacial picture. However, the glacial information provided here is not able to distinguish to what extent each of the previously described mechanisms is responsible.

10.1029/2019PA003613

6.2. Deglaciation

The first change with respect to the ventilation of water masses in the SEP during the deglaciation is the decreased ventilation of intermediate waters (Figures 4, 5, and 7). These changes begin before the deglaciation, around ~19.5 ka cal BP, but become more rapid at ~18.5 ka cal BP at ~540 m, followed by a further depletion at ~800 and ~1,000 m between ~16.5 and 14.5 ka cal BP, while waters at ~1,500 m become better ventilated during the same period. The homogenization of ^{14}C values in the water column in the SEP could be explained by deeper convection of AAIW in the SO during the deglaciation, as proposed by Ronge et al. (2015) in the SWP and Haddam (2016) in the SEP. In fact, a similar change to least ventilated intermediate waters is observed in $\Delta^{14}C$ in the East Pacific margin (Bova et al., 2018) and in the DP (Burke & Robinson, 2012) at depths bathed by southern sourced intermediate waters. Additionally, these changes are paralleled by a shift to $\delta^{13}C$ enriched values between ~16.5 and 14 ka cal BP at ~1,500 m in the SEP (Siani et al., 2013) and at ~1,200 m in the SWP (Sikes et al., 2016) and in the East Pacific margin at ~1,000 m (Bova et al., 2018), which is consistent with increased presence of AAIW at these depths. Around this time, increasing ventilation in deepwater records is also observed in the SA (Skinner et al., 2010), SWP (Ronge et al., 2016; Sikes et al., 2016), EEP (De la Fuente et al., 2015; Umling & Thunell, 2017), and NP (Galbraith et al., 2007; Rae et al., 2014), though not all records show the same trend and timing (Figure 6), maybe denoting local effects and/or inconsistencies in the chronologies of the records. Notably, no increase in ventilation is observed in the SEP in deep waters at ~2,000 m; furthermore, at ~3,000 m even decreased ventilation is observed, a trend contrary to what is observed in most deep ocean records (Figure 6). Unfortunately, no data are available for the whole interval at ~2,000 m to enable a thorough comparison with ~3,000 m waters. The origin of the observed ventilation changes at ~3,000 m is puzzling; they might represent local processes such as reinvigorated mixing of the deep ocean advecting stagnant ^{14}C-depleted deep waters to ~3,000 m or ^{14}C dead-CO_2 injected directly from hydrothermal vents (Judd, 2003), which is likely to have happened due to the numerous active ridges in the area (Beaulieu et al., 2013). Notably, the observed decrease is coeval with the decrease in $\Delta^{14}C$ of intermediate waters in the Galapagos platform (Figure S4), which is thought to be sourced in the NP (Bova et al., 2018). However, this is not observed in deepwater records in the NP or EEP. Thus, the origin for the observed trend remains unknown. A comparable situation is found in waters at ~800 m depth, where one data point displays extremely ^{14}C-depleted values. This situation is not observed in other southern sourced intermediate waters but is similar to what has been observed in Baja California (Lindsay et al., 2015; Marchitto et al., 2007). We have confidence in this value since the ^{14}C dating in this core was performed on the abundance peaks in an area with high sedimentation rates and the resulting value is much larger than the 1σ envelope in all age models (Figure 3). However, given the available information, it is difficult to interpret this particular data point, since a Southern Ocean seems unlikely. Nevertheless, the overall less ventilated and vertically expanded AAIW, together with a generally better ventilated deep ocean between 16.5 and 14.5 ky cal BP, is consistent with an oceanic source for the observed steep decrease in atmospheric ^{14}C at this time (Broecker & Barker, 2007). The ^{14}C records presented here further suggest the ^{14}C-depleted carbon was ventilated from depth in the Southern Ocean.

At shallower intermediate depths (~540 m), we observe a steep decrease in the ^{14}C content earlier in the deglaciation at ~18.5 ka cal BP, around the time of the initial increase in atmospheric pCO_2 in Antarctica (Figure 5; Marcott et al., 2014). A possible explanation relating these observations is sea ice retreat allowing deeper waters to be ventilated and feed the formation of AAIW, as proposed by Ferrari et al. (2014). However, constraints on sea ice extent are very scarce and thus is not yet possible to draw any conclusions on this matter. On the other hand, the decrease in the ^{14}C content at ~800 and ~1,000 m depth, associated with the onset of the inferred deeper convection of AAIW at ~16.5 ka cal BP, is consistent with increased upwelling (Anderson et al., 2009; Siani et al., 2013) and surface water pCO_2 (Martínez-Botí et al., 2015) in the SO. In addition, a migration of the SWW to the south has also been proposed during this time (e.g., Denton et al., 2010; Mohtadi et al., 2008; Moreno et al., 1999) and is inferred from the planktic $\delta^{13}C$ trends in the SEP here presented, as depicted in section 4 (Figure 2). As previously stated, a southern position of the SWW is proposed to increase upwelling of deep waters in the SO (Toggweiler et al., 2006), which might translate to more AAIW formation and sea ice retreat. Unfortunately, even in the modern ocean AAIW formation is not clearly understood (Bostock et al., 2013; McCartney, 1977; Piola & Gordon, 1989; Sloyan et al., 2010), thus, the relation between these processes remains to be clarified. However, recent simulations indicate that the recorded glacial-interglacial changes in carbon species (CO_2, ^{14}C, and ^{13}C) in both the atmosphere and

10.1029/2019PA003613

the ocean could be explained by intensification of the SWW resulting in more AABW and AAIW production (Menviel et al., 2018). An intensification of the SWW would result in steeper isopycnals, allowing AAIW to reach deeper depths near its formation zone, explaining higher $\Delta^{14}C$ values observed in core MD07-3088 and in turn ventilating deeper waters, explaining lower $\Delta^{14}C$ at ~800 and ~1,000 m (Figure 4). Additionally, according to the simulation by Menviel et al. (2018), this deeper convection could allow for an initial upwelling of low-alkalinity intermediate waters, which would be responsible for the observed abrupt CO_2 increase in the atmosphere at ~16 ka cal BP.

The inferred deeper convection of AAIW is interrupted by a brief return to glacial conditions at the beginning of the ACR, in which intermediate waters at ~800 and ~1,000 m become better ventilated and at ~1,500 m less ventilated. This return to a shallower AAIW is brief, and the homogenized ^{14}C values are again observed between ~13.5 and 10.5 ka cal BP. A similar behavior is observed in sea surface pCO_2 in the SO (Martínez-Botí et al., 2015), and both are consistent with the ventilation of deep waters in the SEP at ~2,000 and ~3,000 m. However, these changes are contrasted by constant atmospheric $\Delta^{14}C$ and pCO_2 (Figures 4 and 5). The latter might be explained by problems in the chronology of the records, or it might reflect that even if this process is taking place, it is not dominating the atmospheric signature. Alternatively, from the comparison with deepwater records in Figure 6, it seems plausible that even if deeper convection in the SO was occurring at this time, the larger part of the isolated deepwater reservoir would have been already ventilated; thus, no important increase in atmospheric pCO_2 would have occurred.

The latter might seem inconsistent with the observed increased in atmospheric pCO_2 in ~30 ppm between ~13 and 11.5 ka cal BP. However, it has been proposed that this increase in atmospheric pCO_2 was related to the outgassing in the EEP rather than in the SO (Bova et al., 2018; Martínez-Botí et al., 2015). Extremely ^{14}C-depleted records have been found in the EEP at intermediate water depths (Bova et al., 2018; Stott et al., 2009) and in Baja California (Lindsay et al., 2015; Marchitto et al., 2007) during the deglaciation. Additionally, CO_2 outgassing in the EEP has been reconstructed by Martínez-Botí et al. (2015), which is similar to the observed outgassing in the SO during Heinrich Stadial 1, but ~70 ppm higher during the Younger Dryas (YD). This, together with increased upwelling in the EEP during the YD (Bova et al., 2018), would result in the ventilation of the extremely ^{14}C-depleted intermediate waters and is proposed to be an important contributor to the observed rise in pCO2 (Bova et al., 2018; Martínez-Botí et al., 2015). In addition, simulations indicating the SWW as an important factor in atmospheric pCO_2 increase during the deglaciation only account for ~40 ppm (Menviel et al., 2018; Toggweiler et al., 2006).

Finally, around ~10 ka cal BP the available ^{14}C data indicate the establishment of the current structure, homogeneous deep waters below ~1,500 m, and better ventilated waters above, reaching similar values to the modeled $\Delta^{14}C$ (Figures 4 and 5). The divergence of values at ~1,000 and ~1,500 m with the onset of the Holocene could be interpreted as the end of the conditions that were favoring the deeper convection of the AAIW.

7. Conclusions

The SEP benthic radiocarbon records presented in this study indicate a deepening of AAIW convection during the beginning of the last deglaciation (Haddam, 2016; Ronge et al., 2015). These changes could spur the ventilation of glacial carbon-rich deep waters, contributing to the observed ~40 ppm increase in atmospheric pCO_2 during Heinrich Stadial 1 (Menviel et al., 2018; Toggweiler et al., 2006). This finding of enhanced convection associated with the release of CO_2 through Southern Ocean water masses is consistent with numerous other studies (e.g., Anderson et al., 2009; Bostock et al., 2013; Sloyan et al., 2010), further solidifying this interpretation. The mechanisms for the enhanced convection of AAIW at the beginning of the deglaciation are a subject of debate but could be related to changes in the southern hemisphere westerly winds (e.g., Chiang et al., 2014), perhaps associated with declining Antarctic sea ice extent (Keeling & Stephens, 2001).

During the Younger-Drays period (~13–11 ka cal BP) atmospheric pCO_2 increased by ~30 ppm, but our radiocarbon records suggest a relatively stable pattern of ventilation in the SEP. This suggests that the SO was not the pivotal region for ventilating the second pulse of CO_2 to the atmosphere. Instead, other regions such as the EEP may have provided the conduit for these old waters to the atmosphere, as supported by several radiocarbon records (Stott et al., 2009; Bova et al., 2018; Martínez-Botí et al., 2015).

We observe similarities between our records and those from the EEP (Bova et al., 2018; Stott et al, 2008) both in intermediate and deep waters (Figure S4) that suggest EEP dynamics impact conditions on the Chilean Margin as far south as 46°S and therefore further afield than generally thought. However, the complexity of EEP dynamics, compounded by problems in core chronologies, makes it difficult to draw definitive conclusions on links between the two regions. Future work toward a greater understanding of the interplay between the EEP and SEP is therefore necessary, particularly given that both regions likely play an important role in regulating carbon release from the deep ocean to the atmosphere.

Acknowledgments

We are indebted to the staff of the Keck radiocarbon facility at the University of California, Irvine. We also thank Dra. Silvana Collado, Paola Cárdenas, Andrea Iturra, and Víctor Merino-Campos for laboratory assistance. This work was partially funded by FONDECYT Grants 11100281 and 1140536, Iniciativa Científica Milenio NC-120066, Fondap 15110009 (CR)^2, and ECOS-SUD/CONICYT C15U04. All the data used in this study can be found in the PANGAEA repository (through this link: https://doi.pangaea.de/10.1594/PANGAEA.907746). We also would like to thank the reviewers for the comments on the manuscript, which have enriched the discussion and broaden our view on the issue here addressed.

References

Adkins, J. (2013). The role of deep ocean circulation in setting glacial climates. *Paleoceanography*, *28*, 539–561. https://doi.org/10.1002/palo.20046

Adkins, J., & Boyle, E. (1997). Changing atmospheric Δ^{14}C and the record of deep water paleo-ventilation ages. *Paleoceanography*, *12*(3), 337–344. https://doi.org/10.1029/97PA00379

Adkins, J. F., MacIntyre, K., & Schrag, D. P. (2002). The Salinity, Temperature, and delta δ^{18}O of the Glacial Deep Ocean. *Science*, *298*(5599), 1769–1773. https://doi.org/10.1126/science.1076252

Anderson, R. F., Ali, S., Bradtmiller, L. I., Nielsen, S. H. H., Fleisher, M. Q., Anderson, B. E., & Burckle, L. H. (2009). Wind-driven upwelling in the Southern Ocean and the deglacial rise in atmospheric CO_2. *Science*, *323*(5920), 1443–1448. https://doi.org/10.1126/science.1167441

Barnola, J. M., Raynaud, D., Korotkevich, Y. S., & Lorius, C. (1987). Vostok ice core provides 160,000-year record of atmospheric CO_2. *Nature*, *329*, 408–414. https://doi.org/10.1038/329408a0

Beaulieu, S. E., Baker, E. T., German, C. R., & Maffei, A. (2013). An authoritative global database for active submarine hydrothermal vent fields. *Geochemistry, Geophysics, Geosystems*, *14*, 4892–4905. https://doi.org/10.1002/2013GC004998

Bemis, B. E., Spero, H. J., Bijma, J., & Lea, D. W. (1998). Reevaluation of the oxygen isotopic composition of planktonic foraminifera: Experimental results and revised paleotemperature equations. *Paleoceanography*, *13*(2), 150–160. https://doi.org/10.1029/98PA00070

Blaauw, M., & Christen, A. (2011). Flexible paleoclimate age-depth models using an autoregressive gamma process. *Bayesian Analysis*, *6*(3), 457–c474. https://doi.org/10.1214/11-BA618

Bostock, H., Sutton, P., Williams, M., & Opdyke, B. (2013). Reviewing the circulation and mixing of Antarctic Intermediate Water in the South Pacific using evidence from geochemical tracers and Argo float trajectories. *Deep Sea Research, Part I*, *73*, 84–98. https://doi.org/10.1016/j.dsr.2012.11.007

Bova, S. C., Herbert, T. D., & Altabet, M. A. (2018). Ventilation of northern and southern sources of aged carbon in the eastern equatorial Pacific during the Younger Dryas rise in atmospheric CO_2. *Paleoceanography and Paleoclimatology*, *33*, 1151–1168. https://doi.org/10.1029/2018PA003386

Brink, K. H., Halpern, D., Huyer, A., & Smith, R. L. (1983). The physical environment of the Peru upwelling system. *Progress in Oceanography*, *12*(3), 285–305. https://doi.org/10.1016/0079-6611(83)90011-3

Broecker, W., & Barker, S. (2007). A 190 ‰ drop in atmosphere's Δ^{14}C during the "Mystery Interval" (17.5 to 14.5 kyr). *Earth and Planetary Science Letters*, *256*(1–2), 90–99. https://doi.org/10.1016/j.epsl.2007.01.015

Bryant, S. P., Marchitto, T. M., & Lehman, S. J. (2010). The release of ^{14}C–depleted carbon from the deep ocean during the last deglaciation: Evidence from the Arabian Sea. *Earth and Planetary Science Letters*, *298*(1–2), 244–254. https://doi.org/10.1016/j.epsl.2010.08.025

Burke, A., & Robinson, L. F. (2012). The Southern Ocean's Role in Carbon Exchange During the Last Deglaciation. *Science*, *335*(6068), 557–561. https://doi.org/10.1126/science.1208163

Carré, M., Jackson, D., Maldonado, A., Chase, B., & Sachs, P. (2015). Variability of ^{14}C reservoir age and air-sea flux of CO_2 in the Perú-Chile upwelling region during the past 12,000 years. *Quaternary Research*, *85*(1), 87–93. https://doi.org/10.1016/j.yqres.2015.12.002

Chen, T., Robinson, L. F., Burke, A., Southon, J., Spooner, P., Morris, P. J., & Hong Chin, N. (2015). Synchronous centennial abrupt events in the ocean and atmosphere during the last deglaciation. *Science*, *349*(6255), 1537–1541. https://doi.org/10.1126/science.aac6159

Chiang, J. C. H., Lee, S., Putnam, A. E., & Wang, X. (2014). South Pacific Split Jet, ITCZ shifts, and atmospheric North-South linkages during abrupt climate changes of the last glacial period. *Earth and Planetary Science Letters*, *406*, 233–246. https://doi.org/10.1016/j.epsl.2014.09.012

Crowley, J., Katz, R. F., Huybers, P., Langmuir, C., & Park, S. (2015). Glacial cycles drive variations in the production of oceanic crust. *Science*, *347*(6227), 1237–1240. https://doi.org/10.1126/science.1261508

De la Fuente, M., Skinner, L., Calvo, E., Pelejero, C., & Cacho, I. (2015). Increased reservoir ages and poorly ventilated deep waters inferred in the glacial Eastern Equatorial Pacific. *Nature Communications*, *6*, 7420. https://doi.org/10.1038/ncomms8420

De Pol-Holz, R., Keigwin, L., Southon, J., Hebbeln, D., & Mohtadi, M. (2010). No signature of abyssal carbon in intermediate waters off Chile during deglaciation. *Nature Geoscience*, *3*(3), 192–195. https://doi.org/10.1038/NGEO745

De Pol-Holz, R., Ulloa, O., Lamy, F., Dezileau, L., Sabatier, P., & Hebbeln, D. (2007). Late Quaternary variability of sedimentary nitrogen isotopes in the eastern South Pacific Ocean. *Paleoceanography*, *22*, PA2207. https://doi.org/10.1029/2006PA001308

Denton, G. H., Anderson, R. F., Toggweiler, J. R., Edwards, R. L., Schaefer, J. M., & Putnam, A. E. (2010). The Last Glacial termination. *Science*, *328*(5986), 1652–1656. https://doi.org/10.1126/science.1184119

DeVries, T. (2014). The oceanic anthropogenic CO_2 sink: Storage, air-sea fluxes, and transports over the industrial era. *Global Biogeochemical Cycles*, *28*, 631–647. https://doi.org/10.1002/2013GB004739

DeVries, T., & Primeau, F. (2010). An improved method for estimating water-mass ventilation age from radiocarbon data. *Earth and Planetary Science Letters*, *295*(3–4), 367–378. https://doi.org/10.1016/j.epsl.2010.04.011

Duchamp-Alphonse, S., Siani, G., Michel, E., Beaufort, L., Gally, Y., & Jaccard, S. L. (2018). Enhanced ocean-atmosphere carbon partitioning via the carbonate pump during the last deglacial. *Nature Communications*, *9*(1), 2396. https://doi.org/10.1038/s41467-018-04625-7

Fairbanks, R. G., Sverdlove, M., Free, R., Wiebe, P. H., & Bé, A. W. H. (1982). Vertical distribution and isotopic fractionation of living planktonic foraminifera from the Panama Basin. *Nature*, *298*, 841–844. https://doi.org/10.1038/298841a0

Ferrari, R., Jansen, M. F., Adkins, J. F., Burke, A., Stewart, A. L., & Thompson, A. F. (2014). Antarctic sea ice control on ocean circulation in present and glacial climates. *Proceedings of the National Academy of Sciences of the United States of America*, *111*(24), 8753–8758. https://doi.org/10.1073/pnas.1323922111

Galbraith, E. D., Jaccard, S. L., Pedersen, T. F., Sigman, D. M., Haug, G. H., Cook, M., et al. (2007). Carbon dioxide release from the North Pacific Abyss during the last deglaciation. *Nature*, *449*(7164), 890–893. https://doi.org/10.1038/nature06227

Gersonde, R., Crosta, X., Abelmann, A., & Armand, L. (2005). Sea-surface temperature and sea ice distribution of the Southern Ocean at the EPILOG Last Glacial Maximum—A circum-Antarctic view based on siliceous microfossil records. *Quaternary Science Reviews*, *24*(7–9), 869–896. https://doi.org/10.1002/2014GB004929

Gouretski, V., & Koltermann, K. P. (2004). WOCE global hydrographic climatology (Tech. Rep. 35). Hamburg, Germany: Berichte des Bundesamtes fur Seeschifffahrt und Hydrographie.

Haddam, N. (2016). Rôle de l'Océan Austral dans les Variations Climatiques Rapides de la Dernière Transition Glaciaire-Holocène: Approche Géochimique et Micropaléontologique (Doctoral Thesis). Retrieved from Researchgate. Université Paris-Saclay, France.

Haddam, N. A., Siani, G., Michel, E., Kaiser, J., Lamy, F., Duchamp-Alphonse, S., et al. (2018). Changes in latitudinal sea surface temperature gradients along the Southern Chilean margin since the last glacial. *Quaternary Science Reviews*, *194*, 62–76. https://doi.org/10.1016/j.quascirev.2018.06.023

Hebbeln, D., & cruise participants (2001). PUCK, Report and preliminary results of RV SONNE Cruise SO-156, Valparaíso (Chile) - Talcahuano (Chile), March 29 - May 14, 2001. Bremen, Germany. Berichte, Fachbereich Geowissenschaften, Universität Bremen No. 279.

Hebbeln, D., Lamy, F., Mohtadi, M., & Echtler, H. (2007). Tracing the impact of glacial-interglacial climate variability on erosion of the southern Andes. *Geology*, *35*(2), 131–134. https://doi.org/10.1130/G23243A.1

Holzer, M., Primeau, F. W., DeVries, T., & Matear, R. (2014). The Southern Ocean silicon trap: Data-constrained estimates of regenerated silicic acid, trapping efficiencies, and global transport paths. *Journal of Geophysical Research: Oceans*, *119*(1), 313–331. https://doi.org/10.1002/2013jc009356

Ingram, B., & Southon, J. (1996). Reservoir ages in eastern Pacific coastal and estuarine waters. *Radiocarbon*, *38*(3), 573–582. https://doi.org/10.1017/S0033822200030101

Johnson, R. E. (1973). Antarctic intermediate water in the South Pacific Ocean. In R. Fraser (Ed.), *Oceanography of the South Pacific* (pp. 55–69). Wellington, New Zealand: New Zealand National Commission for UNESCO.

Judd, A. G. (2003). The global importance and context of methane escape from the seabed. *Geo-Marine Letters*, *23*(3–4), 147–154. https://doi.org/10.1007/s00367-003-0136-z

Kaiser, J., Schefuss, E., Lamy, F., Mohtadi, M., & Hebbeln, D. (2008). Glacial to Holocene changes in sea surface temperature and coastal vegetation in north central Chile: High versus low latitude forcing. *Quaternary Science Reviews*, *27*(2122), 2064–2075. https://doi.org/10.1016/j.quascirev.2008.08.025

Keeling, R. (2007). Deglaciation mysteries. *Science*, *316*(5830), 1440–1441. https://doi.org/10.1126/science.1142326

Keeling, R., & Stephens, B. (2001). Antarctic sea ice and the control of Pleistocene climate instability. *Paleoceanography*, *16*(1), 112–131.

Keigwin, L. D., & Lehman, S. J. (2015). Radiocarbon evidence for a possible abyssal front near 3.1 km in the glacial equatorial Pacific Ocean. *Earth and Planetary Science Letters*, *425*, 93–104. https://doi.org/10.1016/j.epsl.2015.05.025

Key, R.M., A. Olsen, S. van Heuven, S. K. Lauvset, A. Velo, X. Lin et al. (2015). Global Ocean Data Analysis Project, Version 2 (GLODAPv2). ORNL/CDIAC-162, NDP-093. Carbon Dioxide Information Analysis Center, Oak Ridge National Laboratory, US Dept. of Energy, Oak Ridge, Tennessee. https://doi.org/10.3334/CDIAC/OTG.NDP093_GLODAPv2.

Kohfeld, K. E., Le Quéré, C., Harrison, S. P., & Anderson, R. F. (2005). Role of marine biology in glacial-interglacial CO_2 cycles. *Science*, *308*(5718), 74–78. https://doi.org/10.1126/science.1105375

Kumamoto, Y., Murata, A., Watanabe, S., & Fukasawa, M. (2011). Temporal and spatial variations on bomb-produced radiocarbon along BEAGLE2003 lines—Revisits of WHP P06, A10, and I03/I04 in the Southern Hemisphere Oceans. *Progress in Oceanography*, *89*(1–4), 49–60. https://doi.org/10.1016/j.pocean.2010.12.007

Lamy, K., Kaiser, J., Ninnemann, U., Hebbeln, D., Arz, H. W., & Stoner, J. (2004). Antarctic timing of surface water changes off Chile and Patagonian ice sheet response. *Science*, *304*(5679), 1959–1962. https://doi.org/10.1126/science.1097863

Latorre, C., De Pol-Holz, R., Carter, C., & Santoro, C. (2017). Using archaeological shell middens as a proxy for past local coastal upwelling in northern Chile. *Quaternary International*, *427*(A), 128–136. https://doi.org/10.1016/j.quaint.2015.11.079

Lindsay, C. M., Lehman, S. J., Marchitto, T. M., Ortiz, J. D. (2015). The surface expression of radiocarbon anomalies near BajaCalifornia during deglaciation. *Earth and Planetary Science Letters*, *422*, 67–74. https://doi.org/10.1016/j.epsl.2015.04.012

Lukas, R. (1986). The termination of the equatorial undercurrent in the eastern Pacific. *Progress in Oceanography*, *16*(2), 63–90. https://doi.org/10.1016/0079-6611(86)90007-8

Lund, D., & Asimow, P. (2011). Does sea level influence mid-ocean ridge magmatism on Milankovitch timescales? *Geochemistry, Geophysics, Geosystems*, *12*, Q12009. https://doi.org/10.1029/2011GC003693

Marchant, M., Hebbeln, D., & Wefer, G. (1998). Seasonal flux patterns of planktic foraminifera in the Peru-Chile Current. *Deep Sea Research, Part I*, *45*(7), 1161–1185. https://doi.org/10.1016/S0967-0637(98)00009-0

Marchitto, T., Scott, J., Ortiz, J., Flückiger, J., & van Green, A. (2007). Marine radiocarbon evidence for the mechanism of deglacial atmospheric CO_2 rise. *Science*, *316*(5830), 1456–1459. https://doi.org/10.1126/science.1138679

Marcott, S. A., Bauska, T. K., Buizert, C., Steig, E. J., Rosen, J. L., Cuffey, K. M., et al. (2014). Centennial-scale changes in the global carbon cycle during the last deglaciation. *Nature*, *514*(7524), 616–619. https://doi.org/10.1038/nature13799

Martínez-Botí, M. A., Marino, G., Foster, G. L., Ziverti, P., Henehan, M. J., Rae, J. W. B., et al. (2015). Boron isotope evidence for oceanic carbon dioxide leakage during the last deglaciation. *Nature*, *518*(7538), 219–222. https://doi.org/10.1038/nature14155

McCartney, M. S. (1977). Subantarctic mode water. *Deep-Sea Research*, *24*, 103–119.

McCartney, M. S. (1982). The subtropical recirculation of mode waters. *Journal of Marine Research*, *40*(Supplement), 427–464.

Menviel, L., Spence, P., Yu, J., Chamberlain, M. A., Matear, R. J., Meissner, K. J., & England, M. H. (2018). Southern Hemisphere westerlies as a driver of the early deglacial atmospheric CO_2 rise. *Nature Communications*, *9*(1), 2503. https://doi.org/10.1038/s41467-018-04876-4

Merino-Campos, V., De Pol-Holz, R., Southon, J., Latorre, C., & Collado-Fabbri, S. (2019). Marine radiocarbon reservoir age along the Chilean continental margin. *Radiocarbon*, *61*(1), 1–16. https://doi.org/10.1017/RDC.2018.81

Mohtadi, M., Hebbeln, D., & Marchant, M. (2005). Upwelling and productivity along the Peru-Chile Current derived from faunal and isotopic compositions of planktic foraminifera in surface sediments. *Marine Geology*, *216*(3), 107–126. https://doi.org/10.1016/j.margeo.2005.01.008

Mohtadi, M., Rossel, P., Lange, C. B., Pantoja, S., Böning, P., Repeta, D. J., et al. (2008). Deglacial pattern of circulation and marine productivity in the upwelling region off central south Chile. *Earth and Planetary Science Letters*, *272*(1-2), 221–230. https://doi.org/10.1016/j.epsl.2008.04.043

Monnin, E., Indermühle, A., Dällenbach, A., Flückiger, J., Stauffer, B., Stocker, T., et al. (2001). Atmospheric CO_2 concentrations over the Last Glacial Maximum. *Science*, *291*(5501), 112–114. https://doi.org/10.1126/science.291.5501.112

Moreno, P. I., Lowell, T. V., Jacobson, G. L. Jr., & Denton, G. H. (1999). Abrupt vegetation and climate changes during the Last Glacial Maximum and last termination in the Chilean Lake District: A case study from Canal de la Puntilla (41°S). *Geografiska Annaler*, *81*(A), 285–311.

Mortyn, P. G., & Charles, C. D. (2003). Planktic foraminiferal depth habitat and $\delta^{18}O$ calibrations: Plankton tow results from the Atlantic sector of the Southern Ocean. *Paleoceanography*, *18*(2), 1037. https://doi.org/10.1029/2001PA000637

Ortiz, J. D., Mix, A. C., & Collier, R. W. (1995). Environmental control of living symbiotic and asymbiotic foraminifera of the California Current. *Paleoceanography*, *10*(6), 987–1009.

Ortiz, J. D., Mix, A. C., Rugh, W., Watkins, J. M., & Collier, R. W. (1996). Deep-dwelling planktonic foraminifera of the northeastern Pacific Ocean reveal environmental control of oxygen and carbon isotopic disequilibria. *Geochimica et Cosmochimica Acta*, *60*(22), 4509–4523. https://doi.org/10.1016/S0016-7037(96)00256-6

Ortlieb, L., Vargas, G., & Saliège, J. F. (2011). Marine radiocarbon reservoir effect along the northern Chile–southern Peru coast (14–24°S) throughout the Holocene. *Quaternary Research*, *75*(1), 91–103. https://doi.org/10.1016/j.yqres.2010.07.018

Otto-Bliesner, B. L., Hewitt, C. D., Marchitto, T. M., Brady, E., Abe-Ouchi, A., Crucifix, M., et al. (2007). Last Glacial Maximum ocean thermohaline circulation: PMIP2 model intercomparisons and data constraints. *Geophysical Research Letters*, *34*, LI2706. https://doi.org/10.1029/2007GL029475

Patrick, A., & Thunell, R. C. (1997). Tropical Pacific sea surface temperatures and upper water column thermal structure during the Last Glacial Maximum. *Paleoceanography*, *12*(5), 649–657.

Pichevin, L. E., Reynolds, B. C., Ganeshram, R. S., Cacho, I., Pena, L., Keefe, K., & Ellam, R. M. (2009). Enhanced carbon pump inferred from relaxation of nutrient limitation in the glacial ocean. *Nature*, *459*(7250), 1114–1117. https://doi.org/10.1038/nature08101

Piola, A. R., & Gordon, A. I. (1989). Intermediate water in the southwestern South Atlantic. *Deep-Sea Research*, *36*(1), 1–16. https://doi.org/10.1016/0198-0149(89)90015-0

Primeau, F. W., Holzer, M., & DeVries, T. (2013). Southern Ocean nutrient trapping and the efficiency of the biological pump, *Journal of Geophysical Research: Oceans*, *118*, 2547–2564. https://doi.org/10.1002/jgrc.20181

Rae, J. W. B., Sarnthein, M., Foster, G. L., Ridgwell, A., Grootes, P. M., & Elliott, T. (2014). Deep water formation in the North Pacific and deglacial CO_2 rise. *Paleoceanography*, *29*, 645–667. https://doi.org/10.1002/2013PA002570

Reid, J. L. (1965). Intermediate waters of the Pacific Ocean. In *The Johns Hopkins Oceanographic Studies, No. 2*. Baltimore, United States of America: The Johns Hopkins Press. 85 p. https://doi.org/10.4319/lo.1966.11.2.0313

Reimer, P. J., Bard, E., Bayliss, A., Beck, J. W., Blackwell, P. G., Ramsey, C. B., et al. (2013). INTCAL13 and MARINE13 radiocarbon age calibration curves 0–50,000 years cal BP. *Radiocarbon*, *55*(4), 1869–1887. https://doi.org/10.2458/azu_js_rc.55.16947

Ronge, T., Tiedemann, R., Lamy, F., Köhler, P., Allway, B. V., Pol-Holz, D., et al. (2016). Radiocarbon constraints on the extent ad evolution of the South Pacific glacial carbon pool. *Nature Communications*, *7*(1), 11487. https://doi.org/10.1038/ncomms11487

Ronge, T. A., Steph, S., Tiedemann, R., Prange, M., Merkel, U., Nürnberg, D., & Kuhn, G. (2015). Pushing the boundaries: Glacial/interglacial variability of intermediate and deep waters in the southwest Pacific over the last 350,000 years. *Paleoceanography*, *30*, 23–38. https://doi.org/10.1002/2014PA002727

Rose, K., Sikes, E., Guilderson, T., Shane, P., Hill, T., Zahn, R., & Spero, H. (2010). Upper-ocean-to-atmosphere radiocarbon offsets imply fast deglacial carbon dioxide release. *Nature*, *466*(7310), 1093–1097. https://doi.org/10.1038/nature09288

Sautter, L. R., & Thunell, R. C. (1991). Planktonic foraminiferal response to upwelling and seasonal hydrographic conditions: Sediment trap results from San Pedro Basin, Southern California Bight. *Journal of Foraminiferal Research*, *21*(4), 347–363. https://doi.org/10.2113/gsjfr.21.4.347

Schlitzer, R. (2018). Ocean Data View software. http://odv.awi.de/.

Siani, G., Michel, E., De Pol-Holz, R., DeVries, T., Lamy, F., Carel, M., et al. (2013). A. Carbon isotope records reveal precise timing of enhanced Southern Ocean upwelling during the last deglaciation. *Nature Communications*, *4*(1), 2758. https://doi.org/10.1038/ncomms3758

Sigman, D. M., & Boyle, E. A. (2000). Glacial/interglacial variations in atmospheric carbon dioxide. *Nature*, *407*(6806), 859–869. https://doi.org/10.1038/35038000

Sikes, E., & Guilderson, T. (2016). Southwest Pacific Ocean surface reservoir ages since the last glaciation: Circulation insights from multiple-core studies. *Paleoceanography and Paleoclimatology*, *3*, 298–310. https://doi.org/10.1002/2015PA002855

Sikes, E. L., Allen, K. A., & Lund, D. (2017). Enhanced $\delta^{13}C$ and $\delta^{18}O$ differences between the South Atlantic and South Pacific during the last glaciation: The deep gateway hypothesis. *Paleoceanography*, *32*, 1000–1017. https://doi.org/10.1002/2017PA003118

Sikes, E. L., Cook, M. S., & Guilderson, T. P. (2016). Reduced deep ocean ventilation in the southern Pacific Ocean during the Last Glaciation persisted into the deglaciation. *Earth and Planetary Science Letters*, *438*, 130–138.

Sikes, E. L., Samson, C. R., Guilderson, T. P., & Howard, W. R. (2000). Old radiocarbon ages in the southwest Pacific Ocean during the last glacial period and deglaciation. *Nature*, *405*(6786), 555–559. https://doi.org/10.1038/35014581

Silva, N., & Fonseca, T. R. (1983). Geostrophic component of the oceanic flow off northern Chile. In P. Arana (Ed.), *Recursos Marinos del Pacífico, Escuela de Ciencias del Mar*, (pp. 59–70). Valparaíso, Chile, Universidad Católica de Valparaíso.

Silva, N., & Neshyba, S. (1977). Corrientes superficiales frente a la costa austral de Chile. *Ciencia y Tecnología del Mar*, *3*, 37–42.

Silva, N., & Neshyba, S. (1980). Masas de agua y circulación geostrófica frente a la costa de Chile Austral. *Serie Científica, Instituto Antártico Chileno*, *25*(26), 5–32.

Silva, N., Rojas, N., & Fedele, A. (2009). Water masses in the Humboldt Current System: Properties, distribution and the nitrate deficit as a chemical water mass tracer for Equatorial Subsurface Water off Chile. *Deep Sea Research, Part II*, *56*(16), 1004–1020. https://doi.org/10.1016/j.dsr2.2008.12.013

Skinner, L., Fallon, S., Waelbroeck, C., Michel, E., & Barker, S. (2010). Ventilation of the deep Southern Ocean and deglacial CO_2 rise. *Science*, *328*(5982), 1147–1151. https://doi.org/10.1126/science.1183627

Skinner, L., McCave, I. N., Carter, L., Fallon, S., Scrivner, A. E., & Primeau, F. (2015). Reduced ventilation and enhanced magnitude of the deep Pacific carbon pool during the last glacial period. *Earth and Planetary Science Letters*, *411*, 45–52. https://doi.org/10.1016/j.epsl.2014.11.024

Sloyan, B. M., Talley, L. D., Chereskin, K., Fine, R., & Holte, J. (2010). Antarctic intermediate water and subantarctic mode water formation in the Southeast Pacific: The role of turbulent mixing. *Journal of Physical Oceanography*, *40*, 1558–1574. https://doi.org/10.1175/2010JPO4114.1

Spero, H. J., & Lea, D. W. (2002). The cause of carbon isotope minimum events on Glacial Terminations. *Science*, *296*(5567), 522–525. https://doi.org/10.1126/science.1069401

Stephens, B. S., & Keeling, R. F. (2000). The influence of Antarctic sea ice in glacial-interglacial CO_2 variations. *Nature*, *404*(6774), 171–174. https://doi.org/10.1038/35004556

Stott, L., Southon, J., Timmermann, A., & Koutavas, A. (2009). Radiocarbon age anomaly at intermediate water depth in the Pacific Ocean during the last deglaciation. *Paleoceanography*, *24*, PA2223. https://doi.org/10.1029/2008PA001690

Stott, L. D., & Timmermann, A. (2011). Hypothesized link between glacial/interglacial atmospheric CO_2 cycles and storage/release of CO_2-rich fluids from deep-sea sediments. In R. Harunur, L. Polyak, & E. Mosley-Thompson (Eds.), *Abrupt climate change: Mechanisms, patterns, and impacts geophysical monograph series*, (Vol. 193, pp. 123–138). United States of America: American Geophysical Union. https://doi.org/10.1029/2010GM001052

Strub, P., Mesías, J., Montecino, V., Rutllant, J., & Salinas, S. (1998). Coastal ocean circulation off western South America Coastal Segment (6,E). In A. Robinson, & K. Brink (Eds.), *The Sea, The Global Coastal Ocean*, (Vol. 11, pp. 272–313). New York: Wiley.

Stuiver, M., & Polach, H. (1977). Reporting of ^{14}C data. *Radiocarbon*, *19*(3), 355–363. https://doi.org/10.1017/S0033822200003672

Sweeney, C., Gloor, E., Jacobson, A. R., Key, R. M., McKinley, G., Sarmiento, J. L., & Wanninkhof, R. (2007). Constraining global air-sea gas exchange for CO_2 with recent bomb ^{14}C measurements. *Global Geochemical Cycles*, *21*, GB2015. https://doi.org/10.1029/2006GB002784

Talley, L. D. (1996). Antarctic Intermediate Water in the South Atlantic. In G. Wefer, W. H. Berger, G. Siedler, & D. J. Webb (Eds.), *The South Atlantic: Present and past circulation*, (pp. 219–238). New York, United States of America: Springer. https://doi.org/10.1007/978-3-642-80353-6_11

Talley, L. D. (1999). Some aspects of ocean heat transport by the shallow, intermediate and deep overturning circulations. In P. U. Clark, R. S. Webb, & L. D. Keigwin (Eds.), *Mechanisms of Global Climate Change at Millennial Time Scales*, *Geophysical Monograph Series* (Vol. 112, pp. 1–22). United States of America: American Geophysical Union. https://doi.org/10.1029/GM112p0001

Talley, L. D. (2013). Closure of the global overturning circulation through the Indian, Pacific, and Southern Oceans: Schematics and transports. *Oceanography*, *26*(1), 80–97. https://doi.org/10.5670/oceanog.2013.07

Taylor, R., & Berger, R. (1967). Radiocarbon content of marine shells from the Pacific coast of central and South America. *Science*, *158*(3805), 1180–1182. https://doi.org/10.1126/science.158.3805.1180-a

Toggweiler, J. R. (1999). Variation of atmospheric CO_2 by ventilation of the ocean's deepest water. *Paleoceanography*, *14*(5), 571–588.

Toggweiler, J. R., Dixon, K., & Broecker, W. S. (1991). The Peru upwelling and the ventilation of the South Pacific thermocline. *Journal of Geophysical Research*, *96*(C11), 20467–20497. https://doi.org/10.1029/91JC02063

Toggweiler, J. R., Russell, J. L., & Carson, S. R. (2006). Midlatitude westerlies, atmospheric CO_2, and climate change during the ice ages. *Paleoceanography*, *21*, PA2005. https://doi.org/10.1029/2005PA001154

Tolstoy, M. (2015). Mid-ocean ridge eruptions as a climate valve. *Geophysical Research Letters*, *42*, 1346–1351. https://doi.org/10.1002/2014GL063015

Tomczak, M., & Godfrey, J. (2003). *Regional oceanography: An introduction*. Delhi: Daya Publishing House. https://doi.org/10.1002/joc.3370150511

Tsuchiya, M., & Talley, L. (1996). Water-property distribution along an eastern Pacific hydrographic section at 135°W. *Journal of Marine Research*, *54*(3), 541–564. https://doi.org/10.1357/0022240963213583

Tsuchiya, M., & Talley, L. (1998). A Pacific hydrographic section at 881W: Water-property distribution. *Journal of Geophysical Research*, *103*(C6), 12899–12918. https://doi.org/10.1029/97JC03415

Umling, N. E., & Thunell, R. C. (2017). Synchronous deglacial thermocline and deep water ventilation in the eastern equatorial Pacific. *Nature Communications*, *8*(1), 1–10. https://doi.org/10.1038/ncomms14203

Watson, A. J., & Naveira Garabato, A. C. (2006). The role of Southern Ocean mixing and upwelling in glacial-interglacial atmospheric CO_2 change. *Tellus Series B: Chemical and Physical Meteorology*, *58*(1), 73–87. https://doi.org/10.1111/j.1600-0889.2005.00167.x

Wiedicke-Hombach M., Andruleit H., Balmaceda G., Bruns A., Contardo X., Cramer B. et al. (2002). SO161 – 5 SPOC (Subduction Processes off Chile) Geologie – Geochemie – Wärmestrom, BGR.

Wooster, W. S., & Gilmartin, M. (1961). The Perú-Chile undercurrent. *Journal of Marine Research*, *19*(3), 97–122.

Wyrtki, K. (1967). Circulation and water masses in the eastern equatorial Pacific Ocean. *International Journal of Oceanography and Limnology*, *1*(2), 117–147.

Zhao, N., & Keigwin, L. D. (2018). An atmospheric chronology for the glacial-deglacial Eastern Equatorial Pacific. *Nature Communications*, *9*(1), 3077. https://doi.org/10.1038/s41467-018-05574-x